AD_____

Award Number: DAMD17-98-1-8147

TITLE: Breast Cancer Screening Using Photonic Technology

PRINCIPAL INVESTIGATOR: Robert R. Alfano, Ph.D.

CONTRACTING ORGANIZATION: Research Foundation of City University of New York
New York, New York 10031

REPORT DATE: September 1999

TYPE OF REPORT: Annual

PREPARED FOR: U.S. Army Medical Research and Materiel Command
Fort Detrick, Maryland 21702-5012

DISTRIBUTION STATEMENT: Approved for Public Release;
Distribution Unlimited

The views, opinions and/or findings contained in this report are those of the author(s) and should not be construed as an official Department of the Army position, policy or decision unless so designated by other documentation.

DTIC QUALITY INSPECTED 4

20001207 045

REPORT DOCUMENTATION PAGE

Form Approved
OMB No. 074-0188

Public reporting burden for this collection of information is estimated to average 1 hour per response, including the time for reviewing instructions, searching existing data sources, gathering and maintaining the data needed, and completing and reviewing this collection of information. Send comments regarding this burden estimate or any other aspect of this collection of information, including suggestions for reducing this burden to Washington Headquarters Services, Directorate for Information Operations and Reports, 1215 Jefferson Davis Highway, Suite 1204, Arlington, VA 22202-4302, and to the Office of Management and Budget, Paperwork Reduction Project (0704-0188), Washington, DC 20503

1. AGENCY USE ONLY (Leave blank)	2. REPORT DATE	3. REPORT TYPE AND DATES COVERED
	September 1999	Annual (15 Aug 98 -14 Aug 99)

4. TITLE AND SUBTITLE
Breast Cancer Screening Using Photonic Technology

5. FUNDING NUMBERS
DAMD17-98-1-8147

6. AUTHOR(S)
Robert R. Alfano, Ph.D.

7. PERFORMING ORGANIZATION NAME(S) AND ADDRESS(ES)
Research Foundation of City University of New York
New York, New York 10031

E-MAIL:alfano@scisun.sci.ccny.cuny.edu

8. PERFORMING ORGANIZATION REPORT NUMBER

9. SPONSORING / MONITORING AGENCY NAME(S) AND ADDRESS(ES)
U.S. Army Medical Research and Materiel Command
Fort Detrick, Maryland 21702-5012

10. SPONSORING / MONITORING AGENCY REPORT NUMBER

11. SUPPLEMENTARY NOTES

12a. DISTRIBUTION / AVAILABILITY STATEMENT
Approved for Public Release;
Distribution Unlimited

12b. DISTRIBUTION CODE

13. ABSTRACT *(Maximum 200 Words)*

The goal of the research is to develop a noninvasive modality that uses non-ionizing near-infrared (NIR) light for imaging and diagnosis of cancerous lesions of human breast. The imaging method involves illuminating the specimen with ultrashort pulses of NIR laser light and construction of images using two approaches: the **shadowgram** method, and the **three dimensional (3-D) inverse reconstruction** method. During this reporting period we set up: (a) **time-sliced imaging** arrangements using an electronic time gate, and optical Kerr gates; (b) a **spectroscopic imaging** arrangement to explore the diagnostic potential of optical methods; and (c) a 3-D inverse reconstruction method that uses the diffusion approximation of the radiative transport theory as the light propagation model, and time-sliced two-dimensional transmitted light intensity data for inversion to obtain images of thick samples. The efficacy of these methods was tested on excised human breast tissues and model scattering media. The time-sliced imaging measurements enabled highlighting of cancerous and normal regions of excised breast tissue specimens. The results of spectroscopic imaging measurements demonstrated the diagnostic potential of optical imaging. Finally, the inverse reconstruction formalism was used to construct 3-D tomographic images of an absorbing object in a model scattering medium.

14. SUBJECT TERMS	15. NUMBER OF PAGES
Breast Cancer, Optical mammography, time-sliced imaging, inverse image reconstruction, shadowgram, spectroscopic imaging	37
	16. PRICE CODE

17. SECURITY CLASSIFICATION OF REPORT	18. SECURITY CLASSIFICATION OF THIS PAGE	19. SECURITY CLASSIFICATION OF ABSTRACT	20. LIMITATION OF ABSTRACT
Unclassified	Unclassified	Unclassified	Unlimited

NSN 7540-01-280-5500

Standard Form 298 (Rev. 2-89)
Prescribed by ANSI Std. Z39-18
298-102

FOREWORD

Opinions, interpretations, conclusions and recommendations are those of the author and are not necessarily endorsed by the U.S. Army.

___ Where copyrighted material is quoted, permission has been obtained to use such material.

___ Where material from documents designated for limited distribution is quoted, permission has been obtained to use the material.

___ Citations of commercial organizations and trade names in this report do not constitute an official Department of Army endorsement or approval of the products or services of these organizations.

N/A In conducting research using animals, the investigator(s) adhered to the "Guide for the Care and Use of Laboratory Animals," prepared by the Committee on Care and use of Laboratory Animals of the Institute of Laboratory Resources, national Research Council (NIH Publication No. 86-23, Revised 1985).

X For the protection of human subjects, the investigator(s) adhered to policies of applicable Federal Law 45 CFR 46.

N/A In conducting research utilizing recombinant DNA technology, the investigator(s) adhered to current guidelines promulgated by the National Institutes of Health.

N/A In the conduct of research utilizing recombinant DNA, the investigator(s) adhered to the NIH Guidelines for Research Involving Recombinant DNA Molecules.

N/A In the conduct of research involving hazardous organisms, the investigator(s) adhered to the CDC-NIH Guide for Biosafety in Microbiological and Biomedical Laboratories.

PI - Signature 9/29/99
Date

(4) TABLE OF CONTENTS

(5) INTRODUCTION

The thrust of the proposed, "**Breast Cancer Screening Using Photonic Technology**" research project is to develop a breast cancer screening modality that uses noninvasive and non-ionizing near-infrared (NIR) light for imaging and diagnosis of cancerous lesions of human breast. The imaging method involves illuminating the specimen with ultrashort NIR pulses of laser light and construction of images using two approaches. The first, known as the **shadowgram** method, utilizes the image bearing component of the forward-transmitted light to form direct shadow images. The second, referred to as the **three dimensional (3-D) inverse reconstruction method,** makes use of the measured transmitted and scattered-light intensity profiles, known or estimated optical properties of the sample, a model for light propagation through turbid media and a sophisticated computer algorithm to construct images of the interior structure of the specimen.

We use a time-sliced detection technique that records a time sequence of two-dimensional (2-D) spatial intensity profiles of light transmitted through the specimen. These 2-D spatial profiles provide direct shadow images for thin samples. Alternatively, and for thick samples, these 2-D profiles are used to reconstruct 3-D images that provide information about the location of the object as well. Tuning the wavelength of imaging light to a known absorption resonance of adipose tissue in a specimen enabled highlighting of the adipose tissue from the fibrous tissue in the specimen. This result demonstrates the diagnostic potential of the **spectroscopic imaging** method.

(6) BODY

The research during the current reporting period proceeded along both the parallel approaches, i.e., the shadowgram method, and the inverse reconstruction technique, and we have major achievements to report in both the arenas. The tasks performed and the progress made may be broadly grouped as follows:

6.1 Setting up and testing of experimental arrangements,

6.2 Development and implementation of the inverse image reconstruction method,

6.3 Time-sliced shadowgram imaging with excised human breast tissues,

6.4 Spectroscopic imaging of excised human breast tissues, and

6.5 Demonstration of 3-D inverse image reconstruction.

We will briefly outline our accomplishments in each of the above five areas, and refer to appended publications (Appendices 1-7) for detailed description where applicable.

6.1 Setting up and Testing of Experimental Arrangements

The major thrust of research in the first year of the **approved** Statement of Work (SOW) was to set up the experimental arrangements for time-sliced imaging [Technical Objectives (TO) 1, 2 and 3; Tasks 1-5]. We have set up the following experimental arrangements for near-infrared shadowgram imaging.

(a) Time-sliced Imaging Arrangement with an Ultrafast Electronic Time Gate: As outlined in **TO 3 (Tasks 5, and 6)** of **SOW,** we have completed the setting up and testing of a time-sliced imaging arrangement. What is even more important is that, we have used the arrangement to obtain time-sliced images of normal and cancerous human breast tissues,[1,2] as well as to reconstruct 3-D inverse images of objects in highly scattering medium.[3,4]

The arrangement uses the output (750-850 nm) of a femtosecond Ti:sapphire laser and amplifier system[5] generating 150 fs, 1 kHz repetition rate, 5 mJ pulses for sample illumination. Time-sliced 2-D images are recorded by an ultrafast gated intensified camera system (UGICS). The UGICS is a compact gated image intensifier unit that is fiber-optically coupled to a CCD camera. It provides an electronic time gate whose FWHM duration may be adjusted to a minimum of approximately 80 ps and the gate position may be varied over a 20-ns range in a minimum step size of 25 ps. **Details of the arrangement is presented in Section 2 of Reference 3 which is included as Appendix 3 of this report.**

(b) Time-sliced Imaging Arrangement with Optical Kerr Gates: Optical Kerr gates (OKGs) hold the promise for providing temporal resolution of a few hundred femtoseconds, the limit being set by the pump pulse duration or the response time of the Kerr medium, whichever is the longest. In order to exploit this high temporal resolution we proposed development of combined OKG, polarization and Fourier space-gated imaging systems (**TO 1, Tasks 1-3**). We have set up and tested (**TO 2, Task 4**) two OKG-based imaging systems.

The first system uses the second harmonic output (400 nm in use but tunable over 375-425 nm) of the Ti:sapphire laser system mentioned above to open the Kerr gate and the fundamental output (800 nm in use, but tunable over 750-850 nm) for imaging, and CS_2 as the Kerr medium. **A schematic diagram of the system is provided in Appendix 5.**

The second system uses the second harmonic output (640 nm in use but tunable over 610-650 nm) of our proprietary Cr:forsterite laser and regenerative amplifier system mentioned above to open the Kerr gate and the fundamental output (1280 nm in use, but tunable over 1220-1300 nm) for imaging, and CS_2 as the Kerr medium. The laser system provides 200 fs, 1 kHz repetition-rate, 50 μJ pulses. **A schematic diagram of the system is provided in Appendix 6.**

Our comparison of the OKG and the UGICS based systems indicates that while the OKG-based system provides higher temporal resolution, the UGICS-based system is more user friendly, easier to implement and provides higher signal since integration over a wider time window is employed.

(c) Spectroscopic Imaging Arrangement: We have assembled a spectroscopic imaging arrangement to explore the diagnostic potential of optical biomedical imaging techniques. It uses the 1210-1300 nm continuous-wave mode-locked output of a Cr:forsterite laser for sample illumination. A Fourier space gate[6] and a polarization gate[7] are used to select the image-bearing photons and discriminate against the multiple-scattered photons. The shadowgram images are recorded by a 128x128 pixels InGaAs NIR area camera (Sensors Unlimited SU-128). **The arrangement is detailed in Section 2 of Reference 2 (Appendix 2) and a schematic diagram is presented in Appendix 7.**

6.2 Development and Implementation of an Inverse Image Reconstruction Method

We have developed[3] a novel inverse image reconstruction (IIR) method that makes use of the sequence of time-sliced 2-D transmitted light intensity distribution measured by the experimental arrangements detailed in Section 6.1 to reconstruct 3-D images of object inside highly-scattering turbid media (**TO 4, Tasks 8, 9**). Diffusion approximation of the radiative transport theory[8] is used to model the light propagation through the turbid media. The formulation of the forward problem assumes a slab geometry described in cylindrical

coordinates. A Green's function perturbative approach under the Rytov approximation[9] is used to produce a linear inverse algorithm. The use in the inversion algorithm of a 2-D matrix inversion with a 1-D Fourier-transform inversion based on the cylindrical symmetry greatly reduces the computation time. The algorithm has been implemented on a Silicon Graphics Origin-2000 computer equipped with 4 parallel 195-MHZ CPU's. **The inverse reconstruction method is detailed in Appendix 3.**

6.3 Time-sliced Shadowgram Imaging with Excised Human Breast Tissues

The efficacy of the time-sliced imaging technique outlined in Section 6.1 was used to obtain shadowgram images of excised human breast tissue specimens (**TO 5-7, Tasks 12, 14**). The specimens were obtained from our collaborators at the Memorial Sloan Kettering Cancer Center and National Disease Research Interchange under an IRB approval at the City College of New York. Specimens with normal and cancerous tissues were used in the experiments. Specimens with infiltrating ductal carcinoma, infiltrating lobular carcinoma, and mucinous carcinoma were investigated.

One of the key results of the study was that light transited through the cancerous tissues faster than through the normal tissue. Consequently, images obtained with light in the earlier time slices highlighted the cancerous tissues, while those obtained with light in the later time slices highlighted the normal tissues. Time-sliced imaging can thus separate out normal and cancerous tissues in excised specimens. **Details of the experimental procedure, results, and time-sliced images are presented in References 1 and 2 (Appendices 1 and 2).**

6.4 Spectroscopic Imaging of Excised Human Breast Tissues

In order to explore the diagnostic potential of optical imaging modalities, (**TO 6, Task 13**) we carried out spectroscopic imaging of excised human breast tissues using the spectroscopic imaging arrangement mentioned in Section 6.1(c). We used excised breast tissue specimens with adipose and fibrous tissues. Shadowgram images were recorded by tuning the Cr:forsterite laser output to (a) 1225 nm close to an adipose tissue absorption resonance,[10] and (b) to wavelengths away from the resonance, such as, 1235, 1245, 1255, 1265, 1275, 1285 and 1300 nm. Marked enhancement in contrast between the adipose and fibrous tissues was observed for the near-resonant image recorded using the 1225-nm light.

The experimental procedure, results, and spectroscopic images are detailed in References 1 and 2 (Appendices 1 and 2). Results of this spectroscopic imaging experiments demonstrate the diagnostic potential of optical imaging.

6.5 Demonstration of 3-D inverse image reconstruction

The ability of the inverse reconstruction method outlined in Section 6.3 to generate 3-D images of an object embedded in a turbid medium using the 2-D time-sliced transmission measurements outlined in Section 6.1(a) was demonstrated (**TO 4, Tasks 8, 9**). The absorbing object was a 3x3x10 mm^3 rectangular parallelepiped made of aluminum and painted black. The scattering medium was Intralipid-10% in water with a reduced scattering coefficient, μ_s' of 0.4 mm^{-1} and an absorption coefficient μ_a of 0.02 mm^{-1}. The Intralipid suspension was contained in a 60 mm long (approximate size of an averaged compressed human breast), 200 mm diameter cylindrical plexiglas cell. The object was suspended on the axis at a distance of 15 mm from the exit surface of the cylindrical cell. Our goal was to obtain 3-D images of the embedded object from time-sliced transmitted intensity measurements.

A sequence of 2-D slices at 100 ps intervals were recorded over a 5-ns range. Three dimensional images of the object with good lateral spatial resolution were obtained. Spatial resolution in the axial direction needed improvement. Simulation using data with different levels of Gaussian distributed noise revealed that noise level in the experimental data may have contributed to the spreading out of the reconstructed image along the axial direction. We are working on reducing the noise level in the experiment and to make the reconstruction algorithm more noise resistant. **The inversion technique and the reconstructed images are detailed in References 3 and 4 (Appendices 3 and 4).**

(7) KEY RESEARCH ACCOMPLISHMENTS

- Demonstrated that time-sliced near-infrared optical imaging enables highlighting of normal and cancerous tissues in excised breast specimens.
- Near-infrared spectroscopic imaging can highlight different types of tissues (such as, adipose and fibrous) when the wavelength of light is tuned to an optical resonance of any of the tissues.

- Results of near-infrared spectroscopic imaging on excised tissues illustrate the diagnostic potential of optical imaging.
- Reconstruction of 3-D images of objects in turbid media from 2-D time-sliced transmission was demonstrated. The method has the potential to provide location of the object in 3-D that is not available from normal x-ray mammography.
- Spectroscopic and time-sliced measurements together have the potential to provide more diagnostic information than other techniques, such as, x-rays.

(8) REPORTABLE OUTCOMES

Articles

1. S. K. Gayen and R. R. Alfano, "Sensing lesions in tissues with light," Opt. Express **4**, 475 (1999).
2. W. Cai, S. K. Gayen, M. Xu, M. Zevallos, M. Alrubaiee, M. Lax, and R. R. Alfano, "Optical tomographic image reconstruction from ultrafast time-sliced transmission measurements," Appl. Opt. **38**, 4237 (1999).
3. S. K. Gayen, M. E. Zevallos, B. B. Das, and R. R. Alfano, "Spectroscopic and time-sliced imaging of human breast tissues," SPIE **3597**, 508 (1999). Proceeding of the SPIE Conference on Optical Tomography and Spectroscopy of Tissue III, 24-28 January 1999, San Jose, California.
4. M. Xu, S. K. Gayen, W. Cai, M. E. Zevallos, M. Lax, and R. R. Alfano, "Time-sliced three dimensional inverse image reconstruction of objects in highly scattering media," SPIE **3597**, 2 (1999). Proceeding of the SPIE Conference on Optical Tomography and Spectroscopy of Tissue III, 24-28 January 1999, San Jose, California.

Abstracts and Presentations

1. M. Xu, S. K. Gayen, W. Cai, M. E. Zevallos, M. Lax, and R. R. Alfano, "Time-sliced three-dimensional inverse image reconstruction of objects in highly scattering media." Presented at SPIE's International Symposium on BiOS '99, Conference 3597: Optical Tomography and Spectroscopy of Tissue III, 24-28 January 1999, San Jose, California.
2. S. K. Gayen, M. E. Zevallos, B. B. Das, and R. R. Alfano, "Near-infrared spectroscopic and time-sliced imaging of human breast tissues." Presented at SPIE's International

Symposium on BiOS '99, Conference 3597: Optical Tomography and Spectroscopy of Tissue III, 24-28 January 1999, San Jose, California.

3. S. K. Gayen, M. E. Zevallos, and R. R. Alfano, "Time-resolved transillumination imaging of normal and cancerous human breast tissues with a picosecond electronic time gate, " Bull. Am. Phys. Soc. **44**, 117 (1999). Paper BC32 7 presented at the Centennial Meeting of the American Physical Society, 20-26 March 1999, Atlanta, Georgia.
4. S. K. Gayen, M. E. Zevallos, and R. R. Alfano, "Time-sliced and spectroscopic near-infrared imaging for cancer detection." Paper CFL4 presented at the Conference on Lasers and Electro-Optics (CLEO '99), May 23-28, Baltimore, Maryland.

Degrees Obtained and Employment Received

The Ph. D. research of Manuel E. Zevallos (U.S. Citizen, Hispanic) entitled, "Near Infrared Optical Imaging and Light Propagation in Highly Scattering Random Media" (defended February 11, 1999) was supported in part by this award and the NASA Institutional Research Award Program. Dr. Zevallos is now employed with IBM.

(9) CONCLUSIONS

The work carried out just in the first year of the award leads to some useful conclusions. **First, time-sliced imaging measurements** reveal that light transits through the cancerous tissues faster than the normal tissues. This feature enables highlighting of cancerous and normal regions of tissues. **Second,** results of **spectroscopic imaging measurements** led to the conclusion that if any tissue had a specific spectroscopic signature (such as, enhanced absorption), then resonant images that exploit that signature can highlight that tissue from other types of tissues. **Finally,** time-sliced 2-D transmission spectroscopic measurements provide a wealth of information for reconstruction of 3-D tomographic images.

"So What Section"

The implication of the first conclusion is that time-sliced imaging offers the possibility of highlighting cancerous lesions in human breast. If the lesion is not too deep into the breast, a direct imaging using backscattering geometry may be possible.

The second conclusion points to the most important potential of optical imaging, that of being able to diagnose the lesion while detecting it. X-ray mammography, the current screening method, can not diagnose cancer.

The final conclusion implies that using time-sliced 2-D transmission measurements 3-D tomographic images of human breast may be obtained.

The research carried out so far lends credence to the original hypothesis that photonic technology has the potential to emerge as a noninvasive modality with diagnostic potential for breast cancer monitoring. Additional funding (federal and corporate) is needed to advance this novel technology.

(10) REFERENCES

1. S. K. Gayen and R. R. Alfano, Opt. Express **4**, 475 (1999).
2. S. K. Gayen, M. E. Zevallos, B. B. Das, and R. R. Alfano, "Spectroscopic and time-sliced imaging of human breast tissues," SPIE **3597**, 508 (1999). Proceeding of the SPIE Conference on Optical Tomography and Spectroscopy of Tissue III, 24-28 January 1999, San Jose, California.
3. W. Cai, S. K. Gayen, M. Xu, M. Zevallos, M. Alrubaiee, M. Lax, and R. R. Alfano, Appl. Opt. **38**, 4237 (1999).
4. M. Xu, S. K. Gayen, W. Cai, M. E. Zevallos, M. Lax, and R. R. Alfano, "Time-sliced three dimensional inverse image reconstruction of objects in highly scattering media," SPIE **3597**, 2 (1999). Proceeding of the SPIE Conference on Optical Tomography and Spectroscopy of Tissue III, 24-28 January 1999, San Jose, California.
5. Q. Fu, F. Seier, S. K. Gayen, and R. R. Alfano, Opt. Lett. **22**, 712 (1997).
6. J. Dolne, K. M. Yoo, F. Liu, and R. R. Alfano, Lasers Life Sci. **6**, 131 (1994).
7. S. G. Demos and R. R. Alfano, Opt. Lett. **21**, 161 (1996).
8. S. R. Arridge, "The forward and inverse problems in time-resolved infrared imaging," in Medical Optical Tomography: Functional Imaging and Monitoring, Vol. IS11 of SPIE Institute Series (SPIE, Bellingham, Washington, 1993).
9. M. A. O'Leary, D. A. Boas, B. Chance, and A. G. Yodh, Opt. Lett. **20**, 426 (1995).
10. F. A. Marks, "Optical determination of the hemoglobin oxygenation state of breast biopsies and human breast cancer xenografts in nude mice," in Proceedings of Physical Monitoring and Early Detection Diagnosis Methods, T. S. Mang and A. Katzir, eds., Proc. SPIE **1641**, 227 (1992).

Appendix 1

Sensing lesions in tissues with light

S. K. Gayen and R. R. Alfano

Institute for Ultrafast Spectroscopy and Lasers, New York State Center for Advanced Technology for Ultrafast Photonic Materials and Applications, Physics Department, The City College and Graduate School of the City University of New York, New York, NY 10031
gayen@scisun.sci.ccny.cuny.edu, alfano@scisun.sci.ccny.cuny.edu

Abstract: The use of light for probing and imaging of biomedical media offers the promise for development of safe, noninvasive, and inexpensive clinical imaging modalities with diagnostic ability. Various properties of light together with the ways it interacts with biological tissues may provide 'multiple windows' to peer inside body organs. Principles and methods for extraction of information about body functions and lesions that capitalize on temporal, spectral, polarization, and spatial characteristics of transmitted light are briefly outlined. As illustrations of the potential and efficacy of light-based techniques, time-sliced and spectroscopic images of normal and cancerous human breast tissues recorded with a femtosecond Ti:sapphire laser and a broadly tunable Cr:forsterite laser, respectively, are presented.
©1999 Optical Society of America
OCIS codes: (170.3880) medical and biological imaging; (170.6920) time-resolved imaging; (290.7050) scattering, turbid media; (999.9999) optical mammography.

References and links

1. For a brief review of different optical imaging techniques see, S. K. Gayen and R. R. Alfano, "Emerging optical biomedical imaging techniques," Opt. Photon. News **7**(3), 17-22 (1996).
2. S. Webb, *The Physics of Medical Imaging*, (Institute of Physics Publishing, Bristol, 1988).
3. M. Cutler, "Transillumination as an aid in the diagnosis of breast lesion," Surg. Gynecol. Obstet. **48**, 721-730 (1929).
4. G. J. Muller, R. R. Alfano, S. R. Arridge, J. Beuthan, E. Gratton, M. Kaschke, B. R. Masters, S. Svanberg and P. van der Zeect (editors), *Medical Optical Tomography: Functional Imaging and Monitoring*, Vol. IS 11, SPIE Institute Series, (SPIE, Bellingham, Washington, 1993).
5. L. Wang, P. P. Ho, C. Liu, G. Zhang and R. R. Alfano, "Ballistic 2-D imaging through scattering wall usin an ultrafast Kerr gate," Science **253**, 769-771 (1991).
6. M. R. Hee, J. Izzat, J. Jacobson, J. G. Fujimoto and E. A. Swanson, "Femtosecond transillumination optica coherence tomography, " Opt. Lett. **18**, 950-952 (1993).
7. M. A. O'Leary, D. A. Boas, B. Chance and A. G. Yodh, "Experimental images of heterogeneous turbid media by frequency-domain diffusing-photon tomography," Opt. Lett. **20**, 426-428 (1995.
8. K. P. Chan, M. Yamada and H. Inaba, "Optical imaging through highly scattering media by use of heterodyne detection in the 1.3-μm wavelength region," Opt. Lett. **20**, 492-494 (1995).
9. K. M. Yoo and R. R. Alfano, "Time-resolved coherent and incoherent components of forward light scattering in random media," Opt. Lett. 15, 320-322 (1990).
10. A. D. Sappey, "Optical Imaging through turbid media with a degenerate four wave mixing correlation time gate," Appl. Opt. **33**, 8346-8353 (1994).
11. S. G. Demos and R. R. Alfano, "Temporal gating in highly scattering media by the degree of optical polarization," Opt. Lett. **21**, 161-163 (1996).
12. D. S. Dilworth, E. N. Leith and J. L. Lopez, "Three-dimensional confocal imaging of objects embedded within thick diffusing media," Appl. Opt. **30**, 1796-1803 (1991).
13. J. J. Dolne, K. M. Yoo, F. Liu and R. R. Alfano, "IR Fourier space gate and absorption imaging through random media," Lasers in Life Sciences **6**, 131-141 (1994).
14. J. A. Moon, P. R. Battle, M. Bashkansky, R. Mahon, M. D. Duncan and J. Reintjes, "Achievable spatial resolution of time-resolved transillumination imaging systems which use multiply scattered light," Phys. Rev. E **53**, 1142-1155 (1996).
15. W. Denk, "Two-photon excitation in functional biological imaging," J. Biomed. Opt. **1**, 296-304 (1996).
16. Y. Guo, P. P. Ho, H. Savage, D. Harris, P. Sacks, S. Schantz, F. Liu, N. Zhadin and R. R. Alfano, "Second harmonic tomography of tissues," Opt. Lett. **22**, 1323-1326 (1997).
17. For a recent review of the inverse reconstruction methods, see S. R. Arridge and J. C. Hebden, "Optical imaging in medicine: II. modeling and reconstruction," Phys. Med. Biol. **42**, 841-853 (1997).

#9627 - $15.00 US
Received April 05, 1999; Revised May 07, 1999
(C) 1999 OSA

18. R. R. Alfano, A. Pradhan, G. C. Tang and S. J. Wahl, "Optical spectroscopic diagnosis of cancer and norma breast tissues," J. Opt. Soc. Am. B **6**, 1015-1023 (1989).
19. R. R. Alfano, C. H. Liu, W. L. Sha, H. R. Zhu, D. L. Akins, J. Cleary, R. Prudente and E. Celmer, "Human breast tissue studied by IR Fourier transform Raman spectroscopy," Laser Life Sci. **4**, 23-28 (1991).
20. R. R. Alfano, S. G. Demos and S. K. Gayen, "Advances in optical imaging of biomedical media," in Annals of the New York Academy of Sciences **820**, 248-271 (1997).
21. S. K. Gayen, M. E. Zevallos, M. Alrubaiee, J. M. Evans and R. R. Alfano, "Two-dimensional near-infrared transillumination imaging of biomedical media with a chromium-doped forsterite laser," Appl. Opt. **37**, 5327-5336 (1998).
22. V. G. Peters, D. R. Wyman, M. S. Patterson and G. L. Frank, "Optical properties of normal and diseased human breast tissues in the visible and near infrared," Phys. Med. Biol. 9, 1317-1334 (1990).
23. F. A. Marks, "Optical determination of the hemoglobin oxygenation state of breast biopsies and human breast cancer xenografts in nude mice," in Proceedings of Physical Monitoring and Early Detection Diagnosis Methods, Thomas S. Mang and Abraham Katzir, eds., Proc. SPIE **1641**, 227-237 (1992).
24. W. Cai, S. K. Gayen, M. Xu, M. Zevallos, M. Alrubaiee, M. Lax and R. R. Alfano, "Optical tomographic image reconstruction from ultrafast time-sliced transmission measurements," Appl. Opt. **38** (to be published).

1. Introduction

Light has unique properties to enable sensing of functions, physiology, and lesions of human body. The past decade has witnessed a rapid growth of research activities to exploit some of those attributes of light for the development of optical biomedical imaging and biopsy techniques [1]. Although an impressive array of body-imaging techniques, such as x-ray imaging, x-ray computed tomography, magnetic resonance imaging, ultrasound, and radioisotope imaging are currently available to yield useful information [2], there are important limitations of safety, resolution, cost, and lack or limited specificity to key chemicals necessary for functional body monitoring. More importantly, conventional techniques sometimes fail to provide necessary information. For example, x-ray mammography, the current 'gold standard' for monitoring breast cancer, is not suitable for imaging dense, young breasts, and may not distinguish between malignant and benign tumors. Optical imaging modalities are being pursued to alleviate most of these limitations and to achieve diagnostic ability through the exploitation of the spectroscopic characteristics of tissues. Consequently, a number of continuous-wave, time-resolved, and frequency-domain optical imaging techniques have evolved over the years [3-16,1]. It should also be noted that any of the above-mentioned imaging techniques provide one type of image only, while by changing the wavelength of light one can obtain multiple images that highlight the various molecular components. In addition, light interacts with biological tissues in a number of different ways providing different means to probe the body.

In this article, we first present a brief overview of the various light-tissue interactions, and the properties of light that enable sensing the interior of body organs, such as breast and prostate. We then illustrate the biomedical sensing potential of light through the time-sliced optical imaging and spectroscopic imaging of normal and cancerous human breast tissues.

2. Background

Shadowgram optical imaging was first attempted in 1929 by Cutler [3] who used white light to illuminate the breast and look for pathology in the transmitted light. Inadequate spatial resolution attainable with the available light sources of that time, and the rapid progress in x-ray mammography eclipsed the development of light-based method, that was also known as transillumination, or, diaphanography [2]. With the advent of broadly tunable near-infrared (NIR) solid-state lasers, such as Ti:sapphire and Cr:forsterite, and the development of charge-coupled device (CCD) and NIR area cameras, there has been a surge in research activities for the development optical body-scanning modalities since the mid-1980's.

#9627 - $15.00 US
(C) 1999 OSA
Received April 05, 1999; Revised May 07, 1999

The *purpose* of an optical body-scanning modality is to identify, locate, and diagnose a 'lesion', such as a tumor, inside human body. The *procedure* involves illuminating the relevant part of the body, such as the breast or the prostate, with bright light of appropriate wavelength and search for indication of pathology in the emergent light. The physical *basis* for the development of an optical modality is the difference between the interaction of light with the lesion and the surrounding tissues. Major *problems* that impede the development include attenuation of light due to scattering and absorption by the tissues, and image blurring due to scattering. The nature and extent of the changes in the properties of light that result from its interaction with biological tissues may be different for normal and diseased tissues, as well as for different types of tissues, and thus provide bases for the development of optical imaging and optical biopsy methods.

The high spectral brightness of laser light makes it the most common choice of researchers for optical biomedical imaging. The enabling attributes of laser light include wavelength, coherence, polarization, pulse duration in the case of mode-locked and Q-switched lasers, intensity and directionality. Each of these properties may change as a result of light-tissue interaction that depends on the wavelength of light. A proper choice of wavelength(s) is a crucial consideration for developing an optical imaging modality. Light in the 'therapeutic window' of 700-1300 nm is less absorbed by the tissue constituents compared to near-ultraviolet, visible, or infrared light and is commonly used for tissue imaging.

The common linear interactions of a beam of light with biological tissues include scattering, absorption, specular and diffuse reflection, and diffuse transmission. Scattering changes the directionality, intensity, coherence, polarization, and pulse-width, of the incident light. Consequently, light transmitted through a scattering medium breaks up into *ballistic*, *snake*, and *diffuse* components [5,9,1]. The early-arriving, forward-propagating ballistic and snake photons carry image information while the multiply-scattered diffuse light blurs the image, and in extreme cases buries it in the background noise. The difference in transit time and changes in the above-mentioned characteristics are exploited for selecting the image-bearing light to form direct transillumination images, or, 'shadowgrams'. Since the image-bearing photons change the least, the idea is to devise a *gate* that will let a significant fraction of the photons with a specific initial property through but block others. Realization of this idea has led to the development of *time*, *coherence*, *polarization*, *nonlinear optical*, and *space* gates [4-16,1]. However, for a highly scattering and thick medium the image-bearing light becomes too weak to form a shadow image. One then resorts to *inverse* methods that make use of the scattered light intensity patterns measured around the object, a mathematical model for description of light propagation in scattering media, and a sophisticated computer algorithm to reconstruct an image of the object [17].

Fluorescence that results from the absorption of light by a molecular constituent, such as tryptophan, tyrosine, collagen, elastin and flavin, of a tissue is a characteristic of that constituent. Changes in the fluorescence spectra, lifetime, intensity, and intensity ratios for different excitation wavelengths may provide markers for lesions and facilitate their imaging [18]. Incident light may be frequency shifted due to Raman scattering by the vibrational modes of the molecular constituents of a tissue and differences in the Raman spectra of normal and diseased tissue may provide diagnostic ability [19]. Nonlinear optical interactions of two photon absorption-induced fluorescence and second harmonic generation have also been used to generate histopathological maps of biological tissues [15,16].

The organs of human body with potential to be investigated by optical spectroscopic techniques include breast, prostate, brain, bladder, bone, cervix, colon, eye, digestive and gynecological tracts, skin, and teeth [20]. The requirements of resolution, penetration depth, diagnostic ability, and specificity to key chemicals of an optical imaging modality depend on the organ and the lesion being investigated.

The remainder of this article focuses on our NIR time-sliced and spectroscopic imaging of human breast tissues *in vitro*. Optical imaging of breast is complicated by the extremely low

#9627 - $15.00 US
Received April 05, 1999; Revised May 07, 1999
(C) 1999 OSA

ratio of image-bearing photons to multiply scattered image-blurring photons, and paucity of high contrast targets that are indicative of the presence of cancer and suitable for imaging. Our thrust is to develop a better understanding of light transport through different types of tissues, obtain NIR transillumination images, and explore the feasibility of distinguishing between normal and cancerous tissues from those images.

3. Materials and Methods

We have investigated excised female human breast tissue specimens with normal fibrous and adipose tissues, as well as normal and cancerous tissues. Types of cancer included infiltrating ductal carcinoma, and infiltrating lobular carcinoma. The tissue specimens were placed between two glass plates and compressed to provide a uniform thickness. The specimens were provided to us by National Disease Research Interchange and Memorial Sloan Kettering Cancer Center under an IRB approval from the City College of New York. Here we present representative results of a time-sliced imaging measurement on a specimen with infiltrating ductal carcinoma, and a spectroscopic imaging measurement on a specimen with adipose and fibrous tissues to demonstrate the potential of optical imaging methods.

The time-sliced imaging approach is an extension of the idea of time-resolved early-light imaging except that picosecond-scale slices of the transmitted light pulse are used to record a sequence of two-dimensional (2D) images for different positions of the time gate. The experimental arrangement made use of 800-nm, 130-fs duration, 1 kHz repetition-rate pulses from a Ti:sapphire laser and amplifier system for sample illumination, and an ultrafast gated intensified camera system (UGICS) for recording 2D images. The UGICS comprised a compact time-gated image intensifier unit fiber-optically coupled to a CCD camera. It provided an approximately 80 ps-duration gate whose position with respect to an external trigger pulse could be varied in a minimum step size of 25-ps over a 20 ns range. The average beam power used in the experiment was approximately 200 mW. The beam was expanded and a 3-cm diameter central part of it was selected out using an aperture to illuminate the sample. The time-sliced images were recorded by the CCD camera for different gate positions and displayed on a personal computer.

The experimental arrangement for NIR spectroscopic imaging, detailed elsewhere [21], made use of 1210-1300 nm continuous-wave mode-locked output of a Cr:forsterite laser to illuminate the sample. A Fourier space gate [13] and a polarization gate [11] were used to select the image-bearing photons. A 50 mm focal-length camera lens placed on the optical axis at a distance of 50 mm from the aperture in the Fourier gate collected and collimated the low-spatial-frequency light filtered by the aperture and directed it to the 128x128 pixels sensing element of an InGaAs NIR area camera. Appropriate neutral density filters were used to maintain the average optical power of the incident beam at approximately 35 mW for all the wavelengths used in the imaging experiment. The laser beam was linearly polarized along the horizontal direction.

4. Results

Time-sliced images of a 5-mm thick breast tissue sample comprising a piece of normal tissue and a cancerous piece with infiltrating ductal carcinoma for two different gate positions are displayed in the left frames of Fig. 1. The zero position was taken to be the time of arrival of the light pulse through a 5-mm thick glass cell filled with water. Corresponding spatial intensity profiles integrated over the same horizontal area for all the images are shown in the frames to the right. The salient feature of the images and intensity profiles is that at early times (25 ps) more light is transmitted through the cancerous region than the normal region, while at a much later time (275 ps) relatively more light arrives through the normal region. Lower scattering or/and higher absorption of light by cancerous tissues may account for the

#9627 - $15.00 US
(C) 1999 OSA
Received April 05, 1999; Revised May 07, 1999
24 May 1999 / Vol. 4, No. 11 / OPTICS EXPRESS 478

observed temporal behavior. Since there is no significant absorption of 800-nm light by the breast tissues, we attribute the observed time-dependent difference in light transmission to the higher scattering of light by the normal tissue than by the cancerous tissue. Although we did not carry out independent measurements of the light transport characteristics of the tissues, our results are consistent with the literature values [22] of reduced scattering coefficient of 1.3 mm^{-1} for normal glandular tissues, and 1 mm^{-1} for cancerous breast tissue at 800 nm. Images recorded with different time slices of the transmitted light could highlight normal and cancerous regions of an excised breast tissue specimen.

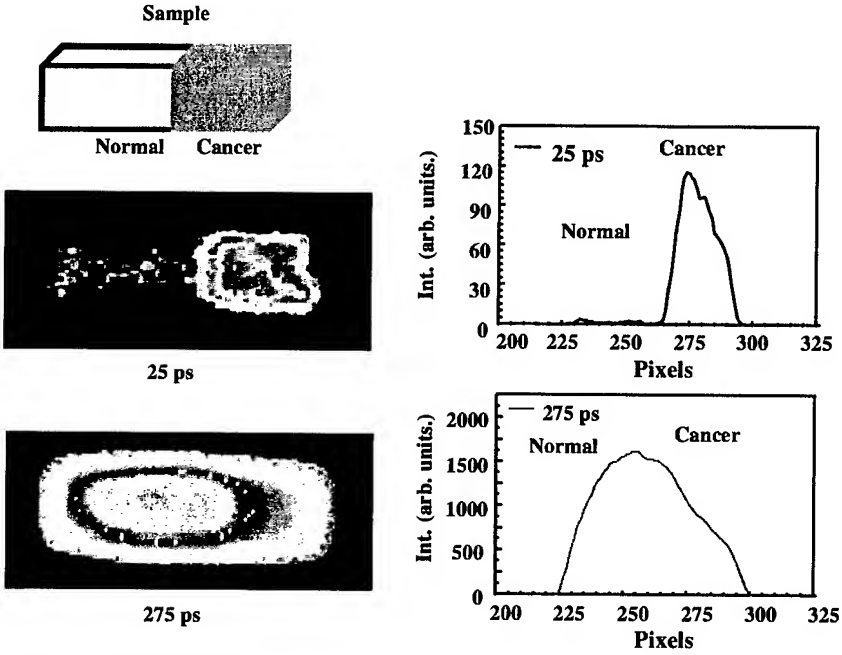

Fig. 1. Time-sliced 2D images (left) of a 25mmx9mmx5mm breast tissue sample with normal and cancerous components for gate positions of 25 ps and 275 ps. Spatial intensity profiles integrated along the same horizontal area are shown in the respective frames to the right. A schematic diagram of the sample is shown in the top left frame. The zero position was taken to be the time of arrival of the light pulse through a 5-mm thick glass cell filled with water.

The thrust of the spectroscopic imaging experiment was to test if a spectroscopic difference between different types of tissues in a specimen provides any distinguishable signature in the transillumination image. We obtained images of a normal breast tissue sample comprising adipose tissue in the middle and fibrous tissues in the two ends with light of wavelengths in the 1225-1300 nm range. Some of the wavelengths were near-resonant with the adipose optical absorption band around 1203 nm, [23] while others were far removed from that resonance. Measurements were made both at the room temperature of 20 ^{0}C and the normal body temperature of 37 ^{0}C. The salient features of the images, displayed in Fig. 2, are: (a) adipose tissue appears much darker (less light transmission) than the fibrous tissues for the near-resonant 1225-nm image as compared to the off-resonance 1285-nm image; and (b) transmission of light through the specimen is higher at 37 ^{0}C than at 20 ^{0}C. Adipose tissue region appeared as a deeper trough in the spatial intensity profile of the 1225-nm image compared to that for the 1285-nm image. For a more quantitative description of the observed behavior, we monitored the image contrast, $C(\lambda,T) = (I_F - I_A)/(I_F - I_A)$, where $I_A(\lambda,T)$ is the optimal intensity value at wavelength λ and temperature T on the spatial profile of the image at the adipose tissue location, and $I_F(\lambda,T)$ is the corresponding intensity at the immediate

#9627 - $15.00 US
Received April 05, 1999; Revised May 07, 1999
(C) 1999 OSA

fibrous tissue region. Values of contrast at 1225 nm are 0.59 and 0.46 for 20 ^{0}C and 37 ^{0}C, respectively, while the corresponding values for 1285 nm are 0.25 and 0.10. As the laser output was tuned away from the absorption peak, the contrast between the adipose and fibrous regions in the images decreased. These results demonstrate that an appreciable spectroscopic difference may significantly enhance the contrast between different types of breast tissues in the transillumination image. The ratio of and/or difference between images recorded with resonant (or near-resonant) light and non-resonant light may enhance the image contrast even further.

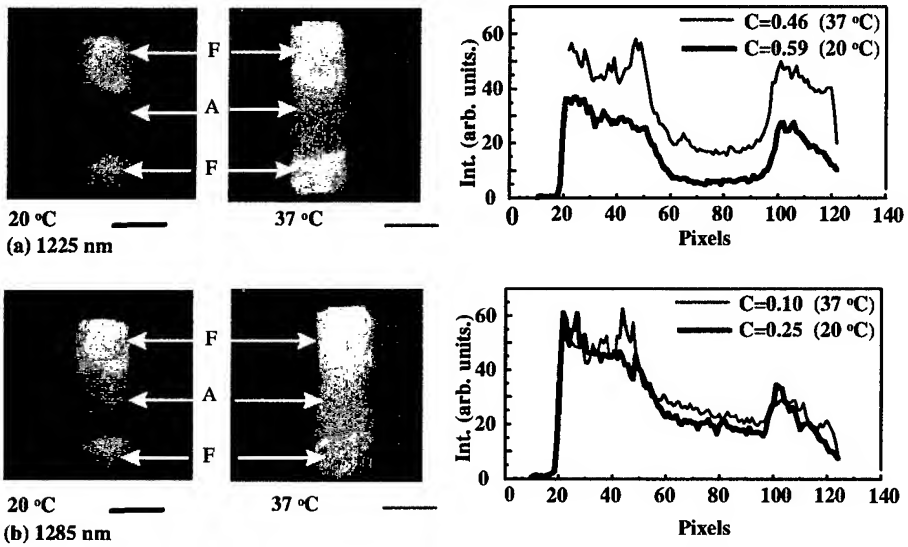

Fig. 2. Spectroscopic 2D images (left frames) of a 28mmx12mmx10mm normal human breast tissue comprising fibrous (F) and adipose (A) components recorded with (a) 1225 nm and (b) 1285 nm light. Spatial intensity profiles of the images integrated over the same vertical area are shown in the respective frames to the right.

5. Discussion

The results of time-sliced imaging experiment demonstrate that optical imaging using optimal time slices of transmitted light is a promising method for imaging biomedical media. While the early-arriving light highlighted the cancerous tissue, the later-arriving light accentuated the normal component. Different types of tissues scatter light differently, and for specific sample configurations the later-arriving light may be as revealing as the early light. Another novel application of the sequence of time-sliced 2D images that is obtained by this approach is in fast three-dimensional tomographic inverse image reconstruction [24]. The time-sliced imaging approach enables fast acquisition of data over a wide frequency range that is necessary for 3D reconstruction, as compared to frequency-domain schemes that commonly use several discrete frequencies.

Results of the NIR spectroscopic imaging experiments demonstrate the diagnostic potential of optical imaging. Combined time-sliced and spectroscopic imaging method has the potential to provide much more information than even the x-ray techniques.

Acknowledgements

We acknowledge M. Zevallos, M. Alrubaiee and J. Evans for technical help. The work is supported by the New York State Science and Technology Foundation, NASA IRA Program, DOE, USAMMRC, and the HEAT program of the City University of New York.

#9627 - $15.00 US Received April 05, 1999; Revised May 07, 1999

(C) 1999 OSA

Appendix 2

Spectroscopic and time-sliced imaging of human breast tissues

S. K. Gayen, M. E. Zevallos, B. B. Das and R. R. Alfano

Institute for Ultrafast Spectroscopy and Lasers, New York State Center for Photonic Materials and Applications, Departments of Physics and Electrical Engineering, The City College of the City University of New York, 138th Street at Convent Avenue, New York, NY 10031

ABSTRACT

Two-dimensional transillumination images of *in vitro* human breast tissue specimens were recorded as a function of the wavelength of near-infrared laser light, as well as, the position of picosecond-duration temporal slices of transmitted light pulse. Spectroscopic imaging arrangement made use of 1225 - 1300 nm light from a chromium-doped forsterite laser for sample illumination, a Fourier space gate and a polarization gate to sort out a fraction of the image-bearing photons, and an InGaAs area camera for recording two-dimensional images. Time-sliced imaging approach used 800-nm, approximately 130-fs duration, 1 kHz repetition-rate pulses from a Ti:sapphire laser system to illuminate the sample, and a gated imaging system that provided a variable-position, ~80 ps-duration electronic gate to record time-sliced two-dimensional images. Excised female breast tissue specimens comprising normal and cancerous, as well as, adipose and fibrous tissues were imaged. Marked enhancement of image contrast between adipose and fibrous tissues in the specimen was observed when the wavelength of imaging light was near-resonant with an absorption band of the human fatty tissue centered on 1203 nm. In time-sliced images, earlier time slices highlighted cancerous tissues, while the later slices accentuated the normal tissues in most of the specimens.

Keywords: Optical mammography; near-infrared absorption spectroscopy of tissues; spectroscopic imaging; transillumination; time-sliced imaging.

1. INTRODUCTION

The article presents the results of spectroscopic and time-sliced transillumination imaging[1-3] measurements on excised human female breast tissue specimens. The thrust of the spectroscopic imaging experiments is to examine if a spectroscopic difference may be used to distinguish between different types of tissues in a specimen. Time-sliced imaging is an extension of the time-resolved early-light imaging except that different temporal slices of the transmitted light intensity profile are used to form images. Images recorded with different temporal slices of the transmitted light is found to selectively highlight different types of tissues, such as, adipose and fibrous or normal and cancerous in excised breast tissue specimens.

2. METHODS AND MATERIALS

The experimental arrangement for near-infrared (NIR) spectroscopic imaging made use of 1210-1300 nm continuous-wave mode-locked output of a Cr^{4+}:forsterite laser to illuminate the sample. A Fourier space gate[4] and a polarization gate[5] were used to select the image-bearing photons and discriminate against the multiple-scattered image-blurring photons. A 50 mm focal-length camera lens placed on the optical axis at a distance of 50 mm from the aperture in the Fourier gate collected and collimated the low-spatial-frequency light filtered by the aperture and directed it to the 128x128 pixels sensing element of an InGaAs NIR area camera. Appropriate neutral density filters were used to maintain the average optical power of the incident beam at approximately 35 mW for all the wavelengths used in the imaging experiment. The laser beam was linearly polarized along the horizontal direction.

The experimental arrangement for time-sliced imaging made use of 800-nm, approximately 130-fs duration, 1 kHz repetition-rate pulses from a self-modelocked Ti:sapphire laser and amplifier system for sample illumination, and an ultrafast electronic gated imaging system (UEGIS) for recording two-dimensional images using picosecond-duration slices

Part of the SPIE Conference on Optical Tomography and Spectroscopy of Tissue III
San Jose, California • January 1999 SPIE Vol. 3597 • 0277-786X/99/$10.00

of the light transmitted through the sample.[6] The UEGIS comprised a compact time-gated image intensifier unit fiber-optically coupled to a charge-coupled device (CCD) camera. It provided an approximately 80 ps-duration gate whose position could be varied in 25-ps steps over a 20-ns range. The average beam power used in the experiment was approximately 200 mW. The beam was expanded by a beam expander, and a 3-cm diameter central part of it was selected out using an aperture to illuminate the sample. The transillumination signal recorded by the system at a particular gate position was a convolution of the transmitted light pulse with the gate pulse centered on the gate position. The time-sliced image was recorded by the CCD camera and displayed on a personal computer.

Excised breast tissue specimens were provided to us by National Disease Research Interchange and Memorial Sloan Kettering cancer center under an IRB approval from the City College of New York. Samples with normal fibrous and adipose tissues, as well as normal and cancerous tissues were studied. Investigated cancerous tissues included those with infiltrating ductal carcinoma, and infiltrating lobular carcinoma with cytologic atypia. The tissue specimens were placed between two glass plates and compressed in an attempt to provide a uniform thickness.

3. RESULTS

To test if a spectroscopic difference between different types of tissues in a specimen provides any distinguishable signature in the transillumination image, we obtained images of a normal sample comprising adipose tissue in the middle and fibrous tissues in the two ends using light of wavelengths that varied from being near-resonant with the adipose optical absorption band around 1203 nm,[7] to being removed from it. Figures 1(a) and 1(b) show 'near-resonant images' recorded using 1225-nm light, and 'nonresonant image' recorded using 1285-nm light, respectively. Measurements were made both at the room-temperature of 20 °C and the body temperature of 37 °C. The salient features of the images are: (a) adipose tissues appear much darker (less light transmission) than the fibrous tissues for the near-resonant 1225-nm image as compared to off-resonance 1285 nm image; and (b) transmission of light through the specimen is higher at 37 °C than at 20 °C. Adipose tissue region appeared as a deeper trough in the spatial intensity profile of the 1225-nm image compared to that for the 1285-nm image. For a more quantitative description of the observed behavior, we monitored the image contrast, $C(\lambda, T) = (I_F - I_A)/(I_F + I_A)$, where $I_A(\lambda,T)$ is the optimal intensity value at wavelength λ and temperature T on the spatial profile of the image at the adipose tissue location, and $I_F(\lambda,T)$ is the corresponding intensity in the immediate fibrous tissue region. Values of contrast at 1225 nm are 0.59 and 0.46 for 20 °C and 37 °C, respectively, while the corresponding values for 1285 nm are 0.25 and 0.10. As the laser output was tuned away from the absorption peak, the contrast between the adipose and fibrous regions in the images decreased. For near-resonant images contrast was higher at 20 °C than at 37 °C. These results clearly demonstrate that an appreciable spectroscopic difference may significantly enhance the contrast between different types of breast tissues in a transillumination image. The ratio of and/or the difference between images recorded using resonant (or near-resonant) and nonresonant light may enhance the image contrast even further.

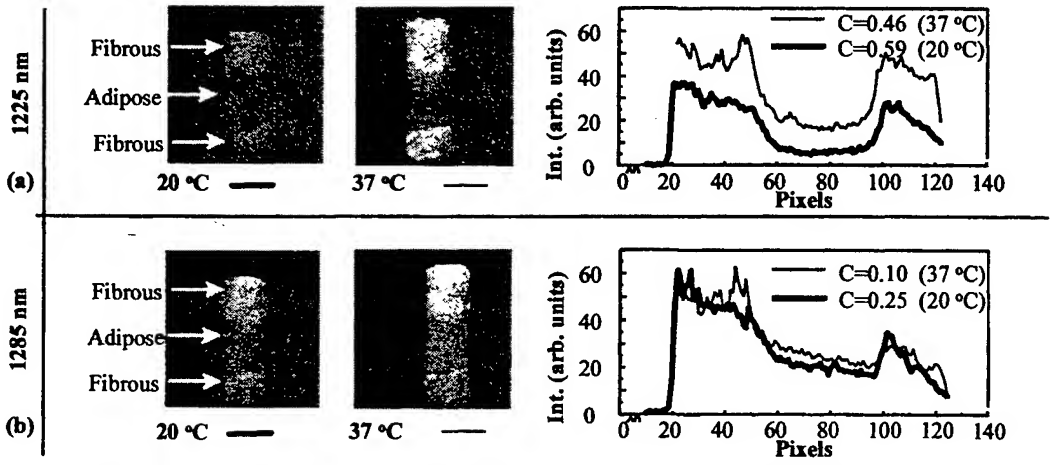

Figure 1. Two-dimensional transillumination images of a 28 mmx12 mmx10 mm human breast tissue sample comprising adipose and fibrous tissues recorded using light of wavelength (a) 1225 nm, and (b) 1285 nm. Spatial intensity profiles of the images integrated over the same vertical area are shown in the rightmost frames.

Time-sliced transillumination images of a 5 mm thick breast tissue sample comprising a piece of normal tissue and a cancerous piece with infiltrating ductal carcinoma for gate positions of 25 and 275 ps are displayed in Figs. 2(a) and 2(b), respectively. The zero position was taken to be the time of arrival of the light pulse through a 5-mm thick glass cell filled with water. The spatial intensity profiles integrated over an horizontal area with a vertical width of 20 pixels are shown in Fig. 2(c). The cancerous and normal regions are clearly distinct in both the 25-ps and the 275-ps images. The spatial intensity distribution of the 25-ps image, displayed by the thin line in Fig. 2(c), shows much higher intensity values in the cancerous region compared to that in the normal region indicating much higher light transmission through the cancerous region at early time. Interestingly, the situation is completely reversed in the spatial intensity profile of the 275-ps image indicated by thick line in Fig. 2(c). Lower scattering or/and higher absorption of light by cancerous tissues may account for the observed temporal behavior. Since there is no known absorption by breast tissue at 800 nm, we attribute the difference in the relative light transmission between the normal and the cancerous human breast tissues at the two different times to the higher scattering of light by the normal tissue. The scattering characteristics of the infiltrating ductal carcinoma sample presented here is different from the highly invasive lobular carcinoma sample with cytologic atypia that we reported in Ref. 6.

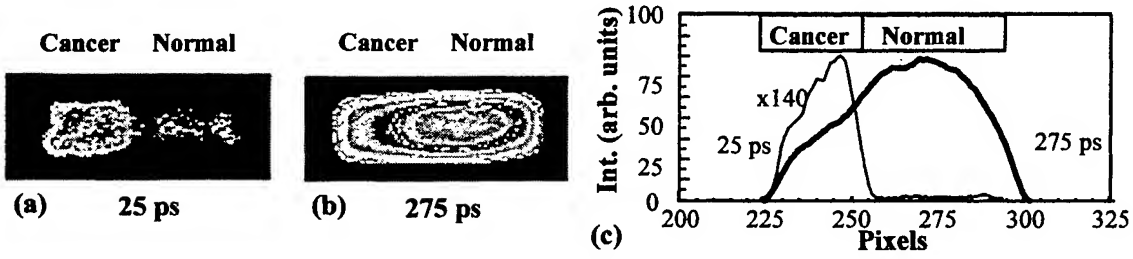

Figure 2. Time-sliced transillumination image of the breast tissue sample described in the text for gate delays of (a) 25, and (b) 275 ps. (c) Spatial profiles of the normalized and integrated intensity distribution along a horizontal area of 20 pixel vertical width of the 25 ps (thick line) and 275 ps (thin line).

In summary, both the spectroscopic and time-sliced imaging methods show tissue selectivity. A combined spectroscopic and time-sliced imaging approach has the potential to provide more information even than the x-ray techniques.

ACKNOWLEDGEMENTS

We acknowledge M. Alrubaiee and J. Evans for technical help. The work is supported by the New York State Science and Technology Foundation, NASA IRA Program, USAMMRC, the HEAT program of the City University of New York, and Mediscience Technology Corp.

REFERENCES

1. L. Wang, P.P. Ho, G. Liu, G. Zhang, and R.R. Alfano, "Ballistic 2-D imaging through scattering walls using an ultrafast optical Kerr Gate", Science **253**, pp. 769-771, 1991.
2. E. Gratton, W. W. Mantulin, M. J. vande Ven, J. B. Fishkin, M. B. Maris, and B. Chance, "A novel approach to laser tomography," Bioimaging, **1**, pp. 40-46, 1993.
3. M. S. Patterson, B. Chance, and B. C. Wilson, "Time resolved reflectance and transmittance for the noninvasive measurement of tissue optical properties," Appl. Opt. **28**, pp. 2331-2336, 1989.
4. J. J. Dolne, K. M. Yoo, F. Liu, and R. R. Alfano, "IR Fourier space gate and absorption imaging through random media," Lasers Life Sci. **6**, pp. 131-141, 1994.
5. S. G. Demos and R. R. Alfano "Temporal gating in highly scattering media by the degree of optical polarization," Opt. Lett. **21**, pp. 161-163, 1996.
6. S. K. Gayen, M. E. Zevallos, B. B. Das, and R. R. Alfano, "Time-sliced transillumination imaging of normal and cancerous breast tissues," in OSA TOPS **21**, *Advances in Optical Imaging and Photon Migration*, edited by J. Fujimoto and M. Patterson, pp. 63-66, 1998.
7. F. A. Marks, "Optical determination of the hemoglobin oxygenation state of breast biopsies and human breast cancer xenografts in nude mice," in *Proceedings of Physiological Monitoring and Early Detection Diagnostic Methods*, Thomas S. Mang and Abraham Katzir (eds.), SPIE **1641**, Bellingham, Washington, pp. 227-237, 1992.

Appendix 3

Optical tomographic image reconstruction from ultrafast time-sliced transmission measurements

W. Cai, S. K. Gayen, M. Xu, M. Zevallos, M. Alrubaiee, M. Lax, and R. R. Alfano

Optical imaging and localization of objects inside a highly scattering medium, such as a tumor in the breast, is a challenging problem with many practical applications. Conventional imaging methods generally provide only two-dimensional (2-D) images of limited spatial resolution with little diagnostic ability. Here we present an inversion algorithm that uses time-resolved transillumination measurements in the form of a sequence of picosecond-duration intensity patterns of transmitted ultrashort light pulses to reconstruct three-dimensional (3-D) images of an absorbing object located inside a slab of a highly scattering medium. The experimental arrangement used a 3-mm-diameter collimated beam of 800-nm, 150-fs, 1-kHz repetition rate light pulses from a Ti:sapphire laser and amplifier system to illuminate one side of the slab sample. An ultrafast gated intensified camera system that provides a minimum FWHM gate width of 80 ps recorded the 2-D intensity patterns of the light transmitted through the opposite side of the slab. The gate position was varied in steps of 100 ps over a 5-ns range to obtain a sequence of 2-D transmitted light intensity patterns of both less-scattered and multiple-scattered light for image reconstruction. The inversion algorithm is based on the diffusion approximation of the radiative transfer theory for photon transport in a turbid medium. It uses a Green's function perturbative approach under the Rytov approximation and combines a 2-D matrix inversion with a one-dimensional Fourier-transform inversion to achieve speedy 3-D image reconstruction. In addition to the lateral position, the method provides information about the axial position of the object as well, whereas the 2-D reconstruction methods yield only lateral position. © 1999 Optical Society of America

OCIS codes: 100.3190, 170.3010, 170.3880, 170.6920, 290.7050.

1. Introduction

The past decade has witnessed a rapid growth of research activities in optical imaging of objects located inside turbid media.[1–12] This interest derives from potential practical applications of optical imaging in such diverse areas as detection of tumors in the human body, monitoring of aerosols and hydrometeors in the atmosphere, and tracking of fuel droplets in the front nozzle of jet engines. Among these areas, biomedical applications have attracted the most attention because safe, noninvasive, and affordable imaging modalities with diagnostic ability can be developed using near-infrared light.[2] An intensely pursued area is optical mammography in which near-infrared light is used to screen for breast cancer, a major and increasing health problem that affects one out of every eight women in the United States.[13] X-ray mammography, the most commonly used breast imaging modality, is not suitable for imaging young dense breasts, may not distinguish between malignant and benign tumors, and frequent exposure to ionizing x rays could be harmful if used for routine screening. The impetus for developing optical mammography is to overcome some of these limitations of x-ray mammography and to achieve diagnostic ability by exploiting potential spectroscopic differences[14,15] between the tumor and the surrounding tissues.

In its simplest form, optical imaging involves illuminating an object with light of appropriate wavelength and looking for its shadow in the transmitted light. Some difference in optical properties between the object and the surrounding medium is necessary for the formation of a shadow image. However, strong scattering of light by biological tissues severely degrades the image quality, and for sufficiently thick tissues, completely buries it in the background noise. Time-

The authors are with the Institute for Ultrafast Spectroscopy and Lasers, New York State Center of Advanced Technology for Ultrafast Photonic Materials and Applications, Departments of Physics and Electrical Engineering, The City College and Graduate Center of City University of New York, New York, New York 10031.

Received 12 November 1998; revised manuscript received 11 March 1999.

0003-6935/99/194237-10$15.00/0

© 1999 Optical Society of America

resolved,[3,5,6,11,12] and continuous-wave (cw)[7,8] methods have been developed to sort out image-bearing ballistic and snake photons from the image-blurring multiple-scattered photons.[16] These methods improve the image quality to different extents, but suffer from low signal-to-noise ratio when used for imaging through thick, highly scattering samples. Inverse image reconstruction (IIR) methods make use of the measured scattered light intensity around the object, knowledge (or estimate) of optical properties of the turbid medium and the object inside it, and mathematical models to construct images of the object.[4,9,12,17–24] An IIR method requires extensive measurement of light intensities around the object and a long computation time for obtaining an image. Continuous-wave or frequency-modulated light, as well as ultrashort light, pulses may be used to accumulate data for IIR.

In this paper we report on a novel IIR approach that makes use of experimentally measured time-sliced two-dimensional (2-D) transmitted light intensity distribution, $I(x, y, t_i)$, to reconstruct three-dimensional (3-D) images. Time-sliced imaging is an extension of the idea of time-resolved early-light imaging except that picoseconds-duration temporal slices of the transmitted light covering both early-arriving less-scattered and late-arriving multiple-scattered photons are used to obtain a sequence of 2-D intensity patterns $I(x, y, t_i)$. Transmission measurements are carried out using a gated image intensifier that provides an approximately 80-ps duration time gate whose temporal position can be varied over a 20-ns range to collect a sequence of 2-D transmitted light intensity distribution $I(x, y, t_i)$. The inversion algorithm uses a 2-D matrix inversion with a one-dimensional (1-D) Fourier-transform inversion based on symmetry in cylindrical coordinates that greatly reduces computation time compared with direct 3-D inversion.

Our approach is a significant advance in optical tomographic imaging of turbid media. First, use of time-resolved data enables reconstruction of 3-D images that provide considerable information about object location in three dimensions. Depth information may not be available from direct transillumination methods, or even x-ray mammography that yields only 2-D images. It has been demonstrated recently that IIR approaches using cw measurements may not be adequate for a unique reconstruction of the internal optical characteristics of a scattering medium even when multiple sources and detectors are used.[25] Shifting of the positions of the source detector pairs may lead to 3-D image information, but it would make data acquisition highly time-consuming. Second, time-sliced data provide a wealth of information over a broad frequency range that is essential for 3-D image reconstruction as compared with frequency-domain schemes that commonly use several discrete frequencies. Frequency-domain methods may, in principle, scan over a broad continuous range of frequencies to generate data that are equivalent to time-domain methods. However, accumulation and processing of data over such a broad frequency range (several gigahertz) would be extremely time-consuming. Moreover, currently available sources cannot provide adequate power at such high frequencies. Use of time-resolved measurements is an effective way to collect data with adequate information content for 3-D image reconstruction.[18] Another advantage of the present scheme that makes use of time-sliced 2-D light intensity patterns over earlier time-domain IIR schemes[17,18] is speedy data acquisition. Those earlier schemes involving measurement of time-resolved profiles using multiple fibers and single-element detectors were time-consuming, expensive, and required complicated synchronization schemes. In the present scheme using a gated charge-coupled device (CCD) camera for detection, each pixel of the 384×288 pixels sensing element can be considered to be equivalent to a detector in the multidetector configuration mentioned above, and a 2-D spatial distribution of transmitted light intensity is obtained in every frame recorded by the camera. Use of only the transmitted light measured with a single CCD camera makes data acquisition simpler and faster than data acquisition that requires measurements of light intensity around the object using multiple detectors. Finally, use of a 2-D matrix inversion with a 1-D Fourier-transform inversion in the algorithm, together with fast time-gated data acquisition, enables reconstruction of 3-D images within a short time, a key requirement for real-time clinical applications. Although the linear perturbative approach has been used before, this use of a 2-D matrix inversion with a 1-D Fourier-transform inversion for speedy image reconstruction is a new salient feature of our approach.

As a proof of concept, we used the method to reconstruct images of an absorbing object placed inside a tissue-simulating model turbid medium. We obtain good localization of the object in the lateral dimensions. Spatial resolution along the axial direction is promising, but needs improvement. The remainder of this paper is organized as follows. Section 2 details the experimental arrangement, sample characteristics, and data-acquisition scheme. The IIR algorithm is presented in Subsection 3.A. Because the inversion problem is ill-posed, some form of regularization is needed to extract useful image information. The degree of regularization is typically controlled by parameters that are usually chosen empirically. The L-curve method[26] that we use to select optimal regularization parameters is described in Subsection 3.B. The formalism is used to reconstruct images of an absorbing object inside a turbid medium and the results are presented in Section 4. The results of reconstruction using simulated data presented in Subsection 4.A is compared with that obtained using experimental data presented in Subsection 4.B. Implications of these results for obtaining tomographic images of biological tissues and the scope of this IIR approach are discussed in Section 5.

2. Experimental Method and Materials

The experimental arrangement for picosecond-duration time-sliced measurement of transmitted light intensity is displayed schematically in Fig. 1(a).

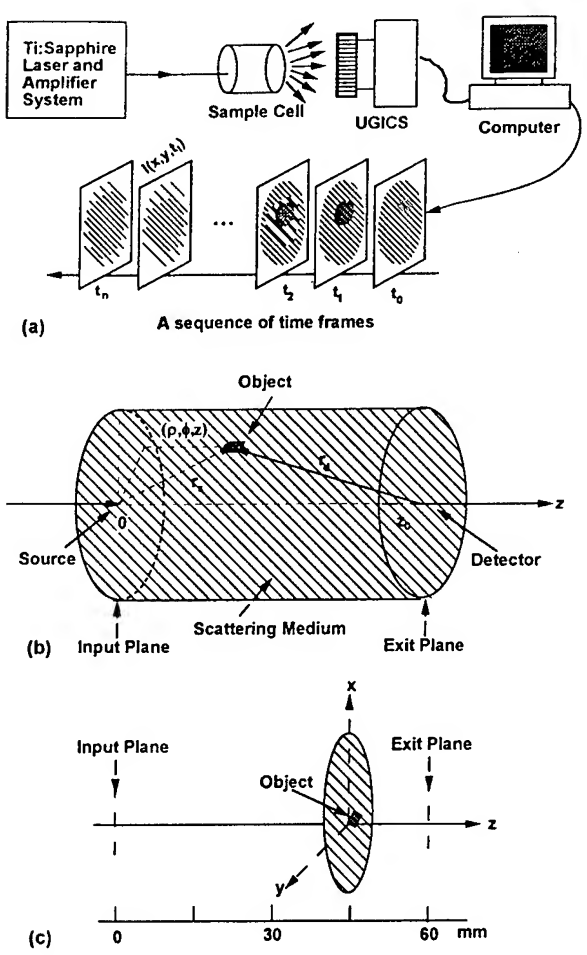

Fig. 1. (a) Schematic diagram of the experimental arrangement used for time-sliced transmitted intensity measurements. (b) Geometric arrangement used to describe the reconstruction algorithm showing the object and image planes and the object in an arbitrary position in cylindrical coordinates. (c) Object location in a lateral plane parallel to and 15 mm away from the exit plane. The 10-mm side of the sample was inclined at an angle of approximately 15° with the vertical (x axis). This is the object position that was used in the experiment.

The detail of the cylindrical sample cell geometry is presented in Fig. 1(b). The location of the object on a plane parallel to and 15 mm toward the source from the exit plane (45 mm from the input plane) is shown in Fig. 1(c). The scattering medium was a suspension of Intralipid-10% (Kabi Pharmacia Inc., Clayton, North Carolina) in water. Intralipid-10% is a fat emulsion used clinically as a nutrient and in research as a phantom to investigate light propagation in tissues. The concentration of Intralipid-10% suspension was adjusted to provide an estimated reduced scattering coefficient μ_s' of 0.4 mm^{-1} and an absorption coefficient μ_a of 0.02 mm^{-1} at 800 nm.[27] The Intralipid suspension was held in a 60-mm-long and 200-mm-diameter cylindrical Plexiglas cell. The cell thickness was chosen to be equivalent to that of an average breast under the extent of compression commonly used in x-ray mammography.

The object to be imaged was a $3 \times 3 \times 10$ mm^3 rectangular parallelepiped made of aluminum and painted black. It was suspended on axis at a distance of 15 mm ($z = 45$ mm) from the exit plane and absorbed most of the light incident on it. The cell was illuminated through the input plane with 150-fs duration, 1-kHz repetition rate pulses of 800-nm light from a Ti:sapphire laser and amplifier system.[28] The 3-mm-diameter collimated laser beam with an average power of approximately 100 mW was incident along the axis (z axis) onto one of the flat faces (input plane) of the cylindrical cell.

The 2-D intensity distribution of light emergent from the opposite endface of the cell (exit plane) was collected by a 24-mm focal-length $f/2.8$ camera lens with a 84° angle of view and was recorded by the ultrafast gated intensified camera system (UGICS). The UGICS is a compact gated image intensifier unit that is fiber optically coupled to a CCD camera. It provides an electronic time gate whose FWHM duration could be adjusted to a minimum of approximately 80 ps. The gate position could be varied over a 20-ns range with a minimum step size of 25 ps. The signal recorded by the system at a particular gate position is a convolution of the transmitted light pulse with the gate pulse centered on the gate position. The collection optics was adjusted to capture light transmitted through the exit plane, and no attempt was made to use the scattered light emergent through the curved surface of the cell. The data then consisted of a sequence of time-resolved 2-D intensity distribution integrated over the gate duration at different gate positions, $I(x, y, t_i)$. Because $I(x, y, t_i)$ is the 2-D spatial intensity distribution integrated over a 80-ps slice of time for the gate position t_i, we refer to it as a time-sliced intensity pattern (or intensity distribution). These time-sliced intensity patterns were recorded by the CCD camera and displayed on a personal computer.

In the experiment reported here, the gate width was adjusted to 80 ps and $I(x, y, t_i)$ were recorded over a 5-ns range by varying the gate pulse position in steps of 100 ps. The zero time was taken to be the instant when the incident light pulse entered the front surface of the cell. $I(x, y, t_i)$ provided the experimental data for IIR.

Experimentally recorded typical 2-D intensity patterns of transmitted light with the object inside the medium are shown in Figs. 2(a) and 2(b) for gate positions of 700 ps and 1500 ps, respectively. The 1500-ps pattern is spatially more spread out than the 700-ps pattern because the electronic time gate collects light that is more diffuse and hence spatially spread out at the 1500-ps position than that at the 700-ps position. Intensity patterns recorded with later gate positions spread out even further. Because the temporal profile of the transmitted light intensity peaks around 2 ns, the intensity at the center of the 1500-ps pattern is higher than that of the 700-ps pattern. No shadow image of the object was apparent in either of the intensity patterns. All the intensity patterns measured over the 5-ns range were

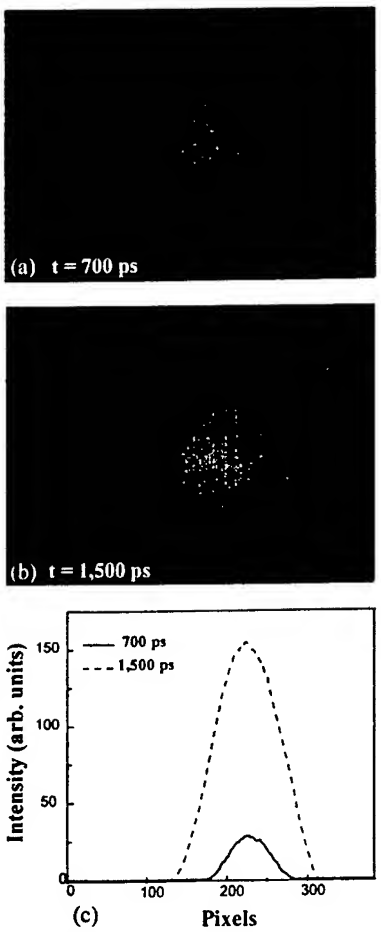

Fig. 2. Experimentally measured 2-D intensity distribution of light transmitted through the scattering medium with the object for a gate position of (a) 700 ps and (b) 1500 ps. (c) The object was located approximately on the axis of the cylindrical cell at a distance of 15 mm from the exit plane.

transferred to a Silicon Graphics Origin-2000 computer for use as experimental data for 3-D IIR. The computer has four parallel 195-MHz CPU's, but only one was used in this research.

3. Reconstruction Formalism

A. Algorithm

The time-sliced IIR formalism presented here is based on the diffusion approximation of the radiative transport theory for photon migration in a scattering medium.[9] The diffusion equation in a turbid medium is given by

$$\left\{\frac{\partial}{\partial t} + \mu_a(\mathbf{r})c - \nabla[D(\mathbf{r})c\nabla]\right\}I(\mathbf{r}, t) = S(\mathbf{r}, t), \quad (1)$$

where I is the photon density (photons/cm^3), S is the source strength [photons/(cm^3·s)], μ_a is the absorption coefficient, $D = 1/\{3[\mu_a + (1 - g)\mu_s]\}$ is the diffusion coefficient, μ_s is the scattering coefficient, g is the scattering anisotropy factor, and c is the speed of light in the medium. We are interested in the following problem: Given the time-sliced intensity pattern transmitted through the media with the object $I(x, y, t_i)$, and without the object $I_0(x, y, t_i)$, we want to reconstruct a map of the change in optical parameters, the absorption coefficient in this case. The medium without the object is referred to as the reference medium.

The formulation of the forward problem uses a slab geometry $(0, z_0)$ formed by cylindrical coordinates (ρ, φ, z), as shown schematically in Fig. 1(b). A point source (or a φ-symmetric finite source) is assumed to be located (or is centered) at (0, 0, 0). The detector system is located on the z_0 plane and is mapped onto the CCD camera by a lens. The ρ boundary is assumed to be at infinity. However, it can be replaced by a finite boundary using a more complex Green's function. We use a Green's function perturbative approach under the Rytov approximation[4,29] to produce a linear inverse algorithm.[9,17] The Rytov approximation is used because it has been shown to provide a more accurate reconstruction of the absorptive properties than the Born approximation.[29] The reference medium, i.e., the medium without the object, is assumed to be uniform. Our formulation requires only the surrounding medium and not the object to be cylindrically symmetric, a condition that can be arranged in an experiment. For example, in the case of breast imaging the breast may be placed in a cylindrical cell containing an index-matching liquid with optical properties that are similar to the average values of optical properties of a real breast. The aim of the reconstruction process would then be to obtain a spatial map of the difference in optical properties from those average values. Thus the assumption of cylindrical symmetry for the surrounding medium is not a serious limitation for the applicability of the formalism.

The forward problem can be represented in matrix form as

$$\mathbf{Y} = W\mathbf{X}, \quad (2)$$

where $\mathbf{Y}$ is a vector represented by a column matrix whose elements are measured changes in transmitted intensity, $\mathbf{X}$ is a vector whose elements are optical parameter (absorption or scattering coefficient) changes that are due to the presence of the object, and W is the weight function,[9] which, in the linear inversion case, is related only to the reference medium. The vector $\mathbf{Y}$ has M elements, determined from the experimental data as $Y_i = -\log(I_i/I_{oi})$, where I_i and I_{oi} are the measured intensities with and without the object, respectively, and $M = (n_t \times n_r \times n_\phi)$ where n_t is the number of time slices and n_r and n_ϕ are the numbers of radial and angular sections, respectively, that the detector plane is divided into. $\mathbf{X}$ has N elements, $X_j = c\Delta\mu_a(\mathbf{r}_j)$ or $c\Delta D(\mathbf{r}_j)$, where N is the number of voxels that the sample cell is divided into. W is an $M \times N$ matrix that, under the assumptions of a cylindrical boundary and a uniform reference medium, satisfies the φ-rotation invariance, i.e., it is a function of $\varphi - \varphi_d$, where φ_d is the angle coordinate of

a point on the detector plane and φ is the angle coordinate of a voxel. It should be pointed out that the reference medium (not the object) needs to be cylindrically symmetric. For time-resolved absorption tomography, W is written as

$$W_{3\text{-D}}(\rho_d, \rho, z, \varphi - \varphi_d t) = \frac{\Delta V}{G_\rho{}^0(\rho_d, t)G_z{}^0(z_0, 0, t)} \times \int_0 d\tau \frac{1}{4\pi Dc(t-\tau)} \times \exp\left[\frac{-\rho^2 - \rho_d{}^2 + 2\rho\rho_d \cos(\varphi - \varphi_d)}{4Dc(t-\tau)}\right] \times G_z{}^0(z, z_0, t-\tau)G_\rho{}^0(\rho, \tau)G_z{}^0(z, 0, \tau). \quad (3)$$

In Eq. (3), $G_z{}^0(z, 0, t)$ is a 1-D slab Green's function for the reference medium with source at $z = 0$ and is written as

$$G_z{}^0(z, 0, t) = (4\pi Dct)^{-1/2} \exp(-z^2/4Dct) + \sum_i (4\pi Dct)^{-1/2} \exp[-(z - z_i)^2/4Dct],$$

where i denotes the ith image source that is due to the slab geometry.

$G_\rho{}^0(\rho, t)$ is a 2-D Green's function with the source located (or centered) at $\rho = 0$. For a point source, it is of the form

$$G_\rho{}^0(\rho, t) = \frac{1}{4\pi Dct} \exp\left(\frac{-\rho^2}{4Dct}\right), \quad (4)$$

and for a finite-size spot source, it is written as

$$G_\rho{}^0(\rho, t) = \frac{1}{2Dct} \int f(\rho_s) \exp\left(-\frac{\rho^2 + \rho_s{}^2}{4Dct}\right) I_0\left(\frac{2\rho\rho_s}{4Dct}\right) \rho_s d\rho_s, \quad (5)$$

where I_0 is the zeroth-order modified Bessel function and $f(\rho_s)$ is the intensity distribution of the incident light spot.

After making a 1-D Fourier transform of $W_{3\text{-D}}$ over $\varphi - \varphi_d$, we obtain K-independent 2-D matrices, $W_{2\text{-D}}(k)$ parameterized by k, with K the number of grid points in the Fourier k space. The indices of $\varphi - \varphi_d$ in the 3-D real space correspond to indices of k in the Fourier space. $W_{2\text{-D}}(k)$ is an $M' \times N'$ matrix, with M' = (number of ρ_d division) $\times$ (number of time slices), and N' = (number of ρ division) $\times$ (number of z division). The normal form $W_{2\text{-D}}(k)^T W_{2\text{-D}}(k)$ is an $N' \times N'$ matrix. We separately calculate the K inverse matrices $[W_{2\text{-D}}(k)^T W_{2\text{-D}}(k) + \Lambda(k)]^{-1}$, $k = 1, 2, \ldots, K$, where $\Lambda(k)$ is a matrix for regularization. The computational complexity now is K times that of inverting a $W_{2\text{-D}}$ matrix, which is much less than that of inverting a $W_{3\text{-D}}$ matrix.

Having experimental data $\mathbf{Y}(\rho_d, \varphi_d, t)$, we make a Fourier transform over φ_d to obtain $\mathbf{Y}(\rho_d, k, t)$, $k = 1, 2, \ldots, K$. The technique for fast discrete Fourier convolution is used. We then use simple matrix multiplication to obtain the image in the k space:

$$\mathbf{X}(k) = \mathbf{Y}(k)^T W_{2\text{-D}}(k)[W_{2\text{-D}}(k)^T W_{2\text{-D}}(k) + \Lambda(k)]^{-1}, \quad k = 1, 2, \ldots K. \quad (6)$$

After $\mathbf{X}(k)$, $k = 1, 2, \ldots K$, is obtained, the inverse 1-D Fourier transform over k reproduces the X as a function of φ and gives the 3-D distribution of the changes in absorption (or scattering) coefficients $\mathbf{X}(\rho, \varphi, z)$.

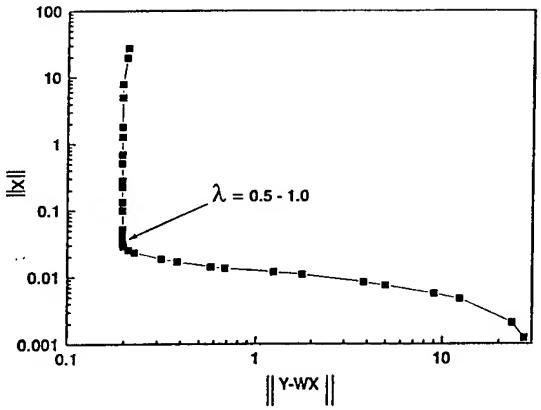

Fig. 3. L curve used for choosing the regularization parameters for IIR with simulated data. The object was located at a distance of 15 mm from the exit plane.

B. Regularization

The inversion problem is ill-posed with a huge condition number, hence a regularization procedure is necessary to obtain a unique solution. We use a diagonal form of a regularization matrix $\Lambda(k) = \lambda(k)\delta_{ij}$. A convenient way to understand the effect of regularization and to choose the suitable regularization parameter is to use the L curve,[26] which shows the properties of the regularized solution $\mathbf{X}_\lambda$ that vary with λ. Two properties of the $\mathbf{X}_\lambda$ are the norm $\|\mathbf{X}_\lambda\|$ and the norm of the corresponding residual vector $\|W\mathbf{X}_\lambda - \mathbf{Y}\|$. $\|\mathbf{X}_\lambda\|$ indicates the stability of the solution and it decreases with an increase of λ. $\|W\mathbf{X}_\lambda - \mathbf{Y}\|$ indicates the error that is due to the introduction of regularization and it increases with an increase of λ. As proved in Ref. 26, if $\|\mathbf{X}_\lambda\|$ versus $\|W\mathbf{X}_\lambda - \mathbf{Y}\|$ is plotted with different values of λ, a curve similar in shape to the capital letter L is obtained. It suggests that a good regularization parameter is one that corresponds to a regularized solution near the corner of the L curve because in this region there is a good compromise that keeps both $\|\mathbf{X}_\lambda\|$ and $\|W\mathbf{X}_\lambda - \mathbf{Y}\|$ relatively small. Figure 3 shows an L curve that we obtained for one of our simulation tests, which corresponded to $W_{2\text{-D}}(k = 1)$. The simulation assumed a Gaussian-distributed noise level with a root-mean-square deviation of 5% (for brevity henceforth referred to simply as 5% Gaussian noise) in each simulated value of Y. The range of the values of λ varies from 10^{-8} to 10^8. The values of λ corresponding to positions near the corner of the L curve are approximately 0.5–1.0. Choice of a value of λ be-

tween 0.5–1.0 in our inversion calculation led to a stable image of the object with the 5% Gaussian noise.

4. Results

A. Three-Dimensional Image from Simulated Data

In the simulation, the thickness of the slab was taken to be $z_0 = 60$ mm. A point light source was assumed. The detector system was taken to be a circle with a radius $R_d = 30$ mm. To choose grids of equal area, the angle 2π was uniformly divided into 36 parts, whereas the radius R_d was divided into 30 parts scaled such that the outer radius of the jth disk was $R_j = (R_d^2 j/J)^{1/2}$, where $j = 1, 2, 3, \ldots, J$, with $J = 30$. In each simulated temporal profile, intensities at 30 time slices uniformly distributed from 450 to 1900 ps were taken. The number of sampling data was $M = 30 \times 36 \times 30$. Data both with and without the object were used to obtain $Y_i = -\log(I_i/I_o)$, after adding the 5% Gaussian noise. The sample cell was divided into $N = 10 \times 36 \times 20$ voxels, with 20 divisions along the z direction and 10 divisions along the ρ direction in a 30-mm range in a way similar to that used for detector division.

Elements of W were calculated using Eq. (3) with a background-reduced scattering coefficient $\mu_s'^0$ of 0.4 mm^{-1} and an absorption coefficient $\mu_a{}^0$ of 0.02 mm^{-1}. Corresponding parameters of the object were $\mu_s' = 0.4$ mm^{-1} and $\mu_a = 0.4$ mm^{-1}. The regularization parameter λ was taken to be 1.0 based on the L-curve analysis. Image of the absorbing object obtained using Eq. (6) and the 1-D Fourier transform is shown in Fig. 3. The 20 consecutive circles in Fig. 4 represent the images at 3-mm intervals along the cylinder axis (z axis) from the input plane to the exit plane. A gray scale is used to display the spatial distribution of changes in the absorption coefficient, with black representing the maximum value. For simulation the object of 3-mm linear dimension was placed in a voxel located in the 15th division along the z axis ($z = 45$ mm) that was approximately 15 mm away from the exit plane.

The reconstructed image locates the object in the neighborhood of where it was placed, as can be seen from the concentration of black around the 15th circle. The image [$\Delta\mu_a(\mathbf{r})$ distribution] appears to be spread out both in the lateral and in the axial directions, a consequence of the scattering and the diffusion approximation used for reconstruction. The FWHM of the image is approximately 6 mm in the lateral plane and approximately 12 mm in the axial direction.

B. Three-Dimensional Image from Experimental Data

In the IIR using experimental data, we approximated the laser beam to be a point source located at the center of the $z_0 = 0$-mm plane. The ρ boundary of the container was assumed to be at infinity. The time-resolved 384 × 288 pixels image from the CCD camera, with and without the object, were transformed to provide $30 \times 36 \times 30$ pieces of $\mathbf{Y}$ data, as

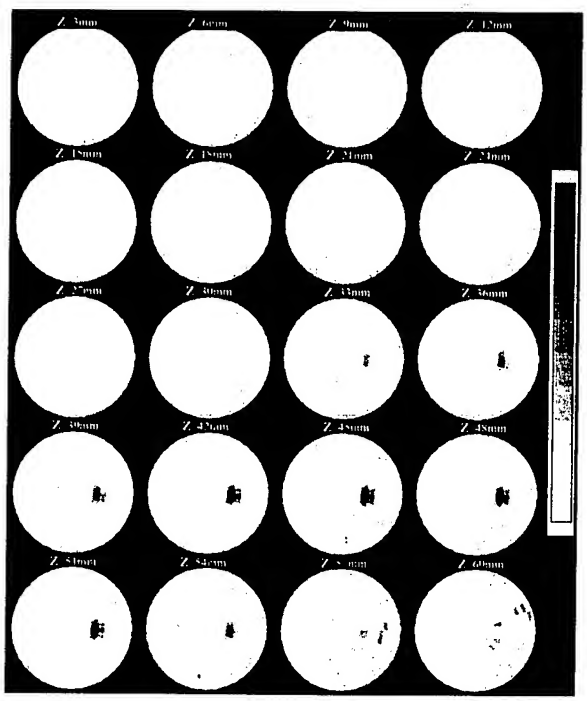

Fig. 4. Images reconstructed from simulated data when the object was located at a distance of 15 mm ($z = 45$ mm) from the exit plane. The sequence of circles represents images at 3-mm intervals along the cylinder axis. The linear intensity scale spans the range 0–20. The maximum value of $\Delta\mu_a(\mathbf{r})$ is 0.04 mm^{-1} and the size of the object is $3 \times 3 \times 3$ mm^3.

was done in simulation. The plot of $\|\mathbf{X}_\lambda\|$ versus $\|W\mathbf{X}_\lambda - \mathbf{Y}\|$ for computing the regularization parameter λ showed only a small kink on the curve instead of a clear L shape. The norm of the residual vector $\|W\mathbf{X}_\lambda - \mathbf{Y}\|$ at kink position was approximately 2 orders of magnitude larger than that in the simulated case. This difference may be due to the deviation of the experimental conditions from the assumptions of the theoretical forward model or because of a higher noise level in the experiment than that used in the simulation. Based on our simulation results assuming higher noise levels, we believe that the difference between the simulated and the experimental results mainly comes from higher experimental noise. Possible sources of experimental noise are pulse-to-pulse energy fluctuation in the laser beam and timing jitter in the gate position. Because we arrange a small object at the distance far enough from the source and the detectors, use of the diffusion equation with the Rytov approximation seems reasonable. Figure 5 shows a 3-D image of the object as a sequence of frames at 3-mm intervals along the axial direction reconstructed using experimental data. The lateral position of the object is reconstructed to be near the cylinder axis in the image map, as one would expect. However, the image is spread out with a half-width of approximately 20 mm along the axial direction. The absorption coefficient distribution appears to be peaked more toward the detector end than the actual object position.

Fig. 5. Images reconstructed from experimental data with the object located at a distance of 15 mm (z = 45 mm) from the exit plane. The sequence of circles represents images at 3-mm intervals along the cylinder axis.

One of the edges of the object was placed on the axis for experimental simplicity only and should not be considered a limitation of the present IIR approach. Reconstruction using simulated data produced a stable solution even when the object was located closer to the cylinder boundary than to the cylinder axis.

5. Discussion

Results of this study indicate that the time-sliced transmission measurements along with the diffusion tomographic IIR method can provide a 3-D map of the location of the object inside a biological tissue-simulating turbid medium. A salient feature of the approach is how short a time it takes for inverse reconstruction. Our estimate shows that a 3-D image of 10 × 36 × 20 voxels can be obtained with a running time of less than 1 min on a Silicon Graphics Origin-2000 computer when only one of its four parallel 195-MHz CPU's is used in the computation. The speed is comparable with that of a 200-MHz Pentium CPU. Combined with a fast data-acquisition scheme that we developed, this algorithm shows the potential for near-real-time IIR.

The reconstructed image of the object has the lateral position that one would expect from the experimental arrangement. The axial position is less certain, as the change in absorption coefficient $\Delta\mu_a(\mathbf{r})$ is more spread out in the axial direction. Comparison with image reconstructed from simulated data indicates that better axial localization is obtained using simulated data than that from the experiment. The position of the object in the reconstructed image gets shifted toward the detector plane for both the simulated and the experimental data. The shift is more pronounced for the image reconstructed using experimental data.

To further investigate this apparent shift in the peak position and the extent of localization, we carried out inverse reconstruction with simulated data (a) for different axial positions of the object and (b) for different noise levels. Reconstructed images using simulated data with a 5% Gaussian noise level for object locations of 30 mm (z = 30 mm) and 45 mm (z = 15 mm) from the exit plane are shown in Figs. 6(a) and 6(b), respectively. Figures 6(a) and 6(b) along with Fig. 4 indicate that, as the object is moved further away from the detector end, its localization in the reconstructed images becomes poorer. The absorption coefficient change $\Delta\mu_a(\mathbf{r})$ spreads out both in the axial and in the lateral directions with a consequent decrease in its peak value as the object distance from the exit plane increases. The result is expected because the further away the object is from the exit plane the higher is the probability for the image-bearing light to spread out and multiply scattered light to encroach into the region of a geometric shadow cast by the absorbing object. The overall effect is a smearing out of the shadow image. The diffusion approximation-based model used here is sensitive to that spreading and reconstructs images whose size and sharpness depend on the object location.

The shift in the peak position of reconstructed $\Delta\mu_a(\mathbf{r})$ distribution toward the exit plane was observed for all three positions of the object. A qualitative explanation for this shift can be given in terms of the dependence of imaging sensitivity on the object location. It is a common observation that for diffuse light imaging, if the object is located on the exit plane it is imaged with minimal distortion and optimal sharpness. Image sharpness decreases and distortion increases as the object is moved further into the scattering medium. Imaging sensitivity is then a function that peaks on the exit plane and gradually decreases toward the input plane. The $\Delta\mu_a(\mathbf{r})$ distribution in the reconstructed image would be proportional to a convolution of this function with $\Delta\mu_a(\mathbf{r})$ distribution of the object and would be shifted toward the exit plane.

The spreading out of the $\Delta\mu_a(\mathbf{r})$ distribution leads to a decrease in its amplitude in the reconstructed image as well because the magnitude of the inhomogeneity gets distributed over a larger region of space. For a small object in three dimensions, the spreading of its image can dramatically decrease the amplitude of imaged optical parameters, in this case $\Delta\mu_a(\mathbf{r})$. This accounts for the peak amplitude of 0.04 mm^{-1} in the reconstructed image of Fig. 4, although the input value of the inhomogeneity was 0.4 mm^{-1}.

Another consequence of the imaging sensitivity being peaked on the exit plane is the observed higher noise level in the z = 60-mm frame (exit plane) of the reconstructed images of Figs. 4, 6(a), and 6(b). The noise in the exit plane seems to be more pronounced

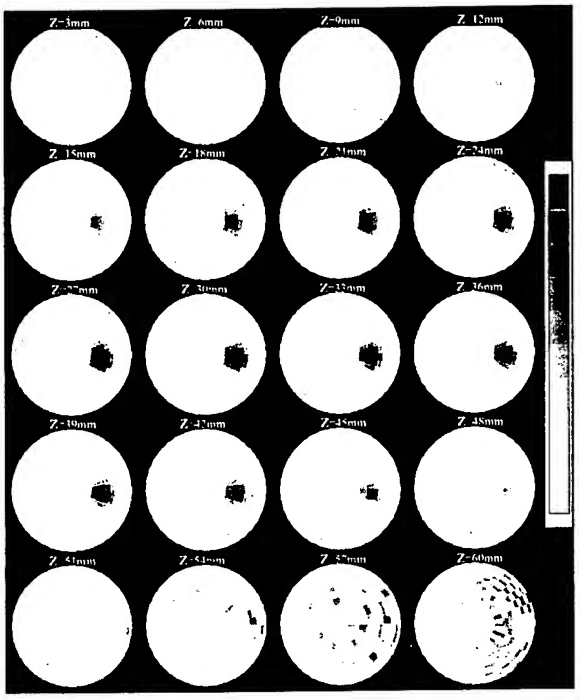

(a)

(b)

Fig. 6. Images reconstructed from simulated data when the object was located at a distance of (a) 30 mm (z = 30 mm) and (b) 45 mm (z = 15 mm) from the exit plane. The sequence of circles represents images at 3-mm intervals along the cylinder axis.

as the object is moved toward the input plane, although the same 5% Gaussian noise level was used for all three cases. The apparent higher noise in Fig. 6(b) is a consequence of the way the $\Delta\mu_a(\mathbf{r})$ distribution is displayed in these figures. The ratio of peak value of $\Delta\mu_a(\mathbf{r})$ to the magnitude of the noise level determines how prominently the noise will be displayed in the scheme used in Figs. 4, 6(a), and 6(b). Because of the object location of 45 mm from the exit plane, the peak value of $\Delta\mu_a(\mathbf{r})$ is much smaller than that of the other two cases, the noise level appears to be more pronounced in the z = 60-mm frame of Fig. 6(b). Simulations with higher noise levels lend support to this observation. With a high enough input noise level, the noise in the exit plane could be as pronounced as the peak value of $\Delta\mu_a(\mathbf{r})$ in the image of the object.

The above observations of peak shift and exit plane noise with simulated data help explain the apparent lower localization and larger shift toward the detector plane of the image from experimental data shown in Fig. 5. We ascribe these to the above-mentioned peaking of imaging sensitivity toward the exit plane and the higher noise level in the experiment compared with the 5% used in simulation. Sources of noise could be energy fluctuation of pulses from the laser amplifier, long-term drift of the laser output, jitters in the position and width of the time gate, and the CCD dark noise. Ample room exists for improvement of the experimental noise and hence object localization. In this proof-of-the-principle experiment, our aim was to test if the algorithm provided meaningful 3-D images from time-sliced 2-D experimental data.

One way of reducing the magnitude of peak shift and improving the localization of the object in the reconstructed image would be to use two sets of data for reconstruction—one taken with the source and detector positioned as described in the text and the second with the z positions of the source and detector reversed. To test this concept, we carried out the reconstruction using the two sets of simulated data as mentioned above for the object position of Fig. 4, that is, 15 mm toward the source from the exit plane. The result, displayed in Fig. 7, shows improvement in object localization when compared with the image in Fig. 4. The improvement will be more substantial for an object located deeper into the scattering medium as a comparison of Fig. 7 with that of Fig. 6(b) reveals.

The IIR scheme presented above would be applicable to imaging of breast *in vivo*. The optical properties, transport parameters, and thickness of the scattering medium used in this experiment are not too far removed from that of breast tissues. Although measurement on the breast with the lesion would provide the signal I, the reference I_0 can be obtained by using a uniform phantom with optical parameters that are equivalent to the average value of the parameters for the breasts. Another interesting possibility is to use measurements using the light of two different but nearby wavelengths. If a wavelength that is resonant with the lesion can be determined, then measurements at that wavelength can be used as the signal and measurements with a nonresonant wavelength can be used as the reference. It should be noted that such lesion-specific wave-

Fig. 7. Images reconstructed from simulated data when the object was located at a distance of 15 mm (z = 45 mm) from the exit plane. Image reconstruction was carried out with data collected using the direct arrangement of both the source and the detector, as well as reversing their positions in the z direction.

lengths are not well established yet. However, our spectroscopic imaging measurements indicate that if the imaging light is tuned into and out of the optical resonance of adipose breast tissues, then the adipose tissues could be highlighted in the transillumination image.[30] Combined spectroscopic and time-sliced measurements may provide much more information for tomographic image reconstruction than that available from single-wavelength x-ray mammography. Identification of fingerprint wavelengths for cancer diagnosis is an actively pursued area of current research. Imaging with such lesion-specific light, if identified, holds the promise for simultaneous detection, localization, and diagnosis of lesions, a unique potential advantage of optical mammography.

One criticism sometimes raised about use of a reference system is that measurements without the object in the reconstruction algorithm need to be addressed. Because our inverse algorithm is linear, the difference in the absorption coefficient between the object and the medium is relevant and the choice of a reference is arbitrary. In principle, it should be possible to reconstruct images from a set of time-sliced measurements on the object in the medium alone and take for the reference medium a uniform background characterized by the average values of optical properties. For example, in an optical mammography application, a uniform medium with values of the optical properties similar to the respective average values of optical properties in the real breast could be considered a reference medium. The algorithm would try to estimate the difference between that assumed background distribution and measurement on the system with the object. The estimation can be carried out as long as the perturbation approach remains valid. Alternatively, only measurements on the object within the medium using two different but nearby wavelengths of light could be used for the signal and reference, as discussed above.

Our IIR method presents a linear approach based on the Rytov approximation, and we were particularly interested in small objects, i.e., weak perturbation. One of the practical reasons for choosing small objects is that breast tumors need to be detected at an early stage of development when they are small in size and are more treatable. Also, the difference in optical properties between normal and cancerous tissues are generally not too large. The magnitude of perturbation depends on the size of both the object and the amplitude of changes in the optical properties between the object and the surrounding medium. The combination is expected to be in the domain of small perturbation for early breast tumors. We considered small objects with high optical contrast that seemed to satisfy the requirements for the linear approach to hold as evident from the stable inverse solutions that we obtained. Linear approaches using frequency-domain measurements were shown to yield inverse images for extended objects by other groups.[4,20,29] The present approach is expected to yield qualitatively adequate results for multiple objects, and extended objects in the strong perturbation limit as well, although the details of the object shape and amplitude of optical parameter changes may not be quantitatively precise. However, at the current state of development, similar limitations are shared by other linear and nonlinear approaches as well. The advantages of the present linear approach are speed of reconstruction, ability to provide 3-D images, and generation of stable solutions without the need for artificial termination of iteration to avoid divergence that is needed for nonlinear methods. Unlike nonlinear iterative methods,[22,23] the linear approach is more susceptible to producing erroneous results for large and strong objects.

In summary, even with the above-mentioned caveats and present limitations, the wavelength-dependent, time-sliced transmission measurements and the diffusion tomographic inverse algorithm show promise for providing 3-D images of objects in a turbid medium, such as a tumor in a breast within a clinically acceptable time frame.

This research is supported in part by the National Aeronautics and Space Administration, the U.S. Army Medical and Materiels Research Command, the Mediscience Technology Corp., and the New York State Science and Technology Foundation.

References and Notes

1. For a brief review of optical imaging techniques, see S. K. Gayen and R. R. Alfano, "Emerging optical biomedical imaging techniques," Opt. Photon. News **7**(3), 16–22 (1996).

2. G. J. Muller, R. R. Alfano, S. R. Arridge, J. Beuthan, E. Gratton, M. Kaschke, B. R. Masters, S. Svanberg, and P. van der Zeeet, eds., *Medical Optical Tomography: Functional Imaging and Monitoring*, Vol. IS 11 of SPIE Institute Series (SPIE, Bellingham, Wash., 1993).
3. L. Wang, P. P. Ho, C. Liu, G. Zhang, and R. R. Alfano, "Ballistic 2-D imaging through scattering wall using an ultrafast Kerr gate," Science **253,** 769–771 (1991).
4. M. A. O'Leary, D. A. Boas, B. Chance, and A. G. Yodh, "Experimental images of heterogeneous turbid media by frequency-domain diffusing-photon tomography," Opt. Lett. **20,** 426–428 (1995), and relevant references therein.
5. R. R. Alfano, X. Liang, L. Wang, and P. P. Ho, "Time-resolved imaging of translucent droplets in highly scattering turbid media," Science **264,** 1913–1915 (1994).
6. M. R. Hee, J. Izzat, J. Jacobson, J. G. Fujimoto, and E. A. Swanson, "Femtosecond transillumination optical coherence tomography," Opt. Lett. **18,** 950–952 (1993).
7. M. Cutler, "Transillumination as an aid in the diagnosis of breast lesion," Surg. Gynecol. Obstet. **48,** 721–730 (1929).
8. A. O. Wist, P. P. Fatouros, and S. L. Herr, "Increased spatial resolution in transillumination using collimated light," IEEE Trans. Med. Imaging **12,** 751–757 (1993).
9. S. R. Arridge, "The forward and inverse problems in time-resolved infrared imaging," in *Medical Optical Tomography: Functional Imaging and Monitoring*, Vol. IS 11 of SPIE Institute Series (SPIE, Bellingham, Wash., 1993).
10. E. Gratton, W. Mantolin, M. vande Ven, J. Fishkin, M. Maris, and B. Chance, "A novel approach to optical tomography," Bioimaging **1,** 40–46 (1993), pp. 35–64.
11. E. B. de Haller, "Time-resolved transillumination and optical tomography," J. Biomed. Opt. **1,** 7–17 (1996).
12. J. C. Hebden, S. R. Arridge, and D. T. Deply, "Optical imaging in medicine: I. Experimental techniques," Phys. Med. Biol. **42,** 825–840 (1997); S. R. Arridge and J. C. Hebden, "Optical imaging in medicine: II. Modelling and reconstruction," Phys. Med. Biol. **42,** 841–853 (1997).
13. E. Marshall, "Search for a killer: focus shifts from fat to hormones in a special report on breast cancer," Science **259,** 618–621 (1993).
14. R. R. Alfano, A. Pradhan, G. C. Tang, and S. J. Wahl, "Optical spectroscopic diagnosis of cancer and normal breast tissues," J. Opt. Soc. Am. B **6,** 1015–1023 (1989).
15. M. S. Feld, R. Manoharan, J. Salenius, J. Ornstein-Carndona, T. J. Romer, J. F. Brennan III, R. R. Dasari, and Y. Wang, "Detection and characterization of human tissue lesions with near-infrared Raman spectroscopy," in *Advances in Fluorescence Sensing Technology II*, J. R. Lakowicz, ed., Proc. SPIE **2388,** 99–104 (1995).
16. K. M. Yoo and R. R. Alfano, "Time-resolved coherent and incoherent components of forward light scattering in random media," Opt. Lett. **15,** 320–322 (1990). For a discussion of the characteristics of photons transmitted through a turbid medium, see Refs. 1 and 12 and relevant references in those papers.
17. W. Cai, B. B. Das, F. Liu, M. Zevallos, M. Lax, and R. R. Alfano, "Time-resolved optical diffusion tomographic image reconstruction in highly scattering turbid media," Proc. Natl. Acad. Sci. USA **93,** 13561–13564 (1996).
18. W. Cai, B. B. Das, F. Liu, Fan An Zeng, M. Lax, and R. R. Alfano, "Three-dimensional image reconstruction in highly scattering turbid media," in *Proceedings of Optical Tomography and Spectroscopy of Tissue: Theory, Instrumentation, Model, and Human Studies II*, B. Chance and R. R. Alfano, eds., Proc. SPIE **2979,** 241–248 (1997).
19. J. Singer, F. Grunbaum, P. Kohn, and J. Zubelli, "Image reconstruction of the interior of the bodies that diffuse radiation," Science **248,** 990–992 (1990).
20. H. Jiang, K. D. Paulsen, U. L. Osterberg, B. W. Pogue, and M. S. Patterson, "Optical image reconstruction using frequency-domain data: simulations and experiments," J. Opt. Soc. Am. A **13,** 253–266 (1996).
21. S. B. Colak, D. G. Papaioannou, G. W. 't Hooft, M. B. van der Mark, H. Schomberg, J. C. J. Paasschens, J. B. M. Melissen, and N. A. A. J. van Asten, "Tomographic image reconstruction from optical projections in light-diffusing media," Appl. Opt. **36,** 180–213 (1997).
22. A. H. Hielscher, A. Klose, D. Catarious, Jr., and K. Hanson, "Tomographic imaging of biological tissue by time-resolved model-based iterative image reconstruction," in *Advances in Optical Imaging and Photon Migration*, J. G. Fujimoto and M. S. Patterson, eds., Vol. 21 of 1998 OSA Trends in Optics and Photonics (1998), pp. 156–161.
23. H. Jiang "Three-dimensional optical image reconstruction: finite element approach," in *Advances in Optical Imaging and Photon Migration*, J. G. Fujimoto and M. S. Patterson, eds., Vol. 21 of 1998 OSA Trends in Optics and Photonics (1998), pp. 168–170.
24. C. L. Matson, N. Clark, L. McMackin, and J. S. Fender, "Three-dimensional tumor localization in thick tissue with the use of diffuse photon-density waves," Appl. Opt. **36,** 214–220 (1997).
25. S. R. Arridge and W. R. B. Lionheart, "Nonuniqueness in diffusion-based optical tomography," Opt. Lett. **23,** 882–884 (1998).
26. P. C. Hansen, "Analysis of discrete ill-posed problems by means of the *L* curve," SIAM (Soc. Ind. Appl. Math.) Rev. **34,** 561–580 (1992).
27. H. J. van Staveren, C. J. M. Moes, J. van Marle, S. A. Prahl, and M. J. van Gemert, "Light scattering in Intralipid-10% in the wavelength range of 400–1100 nm," Appl. Opt. **30,** 4507–4514 (1991).
28. Q. Fu, F. Seier, S. K. Gayen, and R. R. Alfano, "High-average-power, kilohertz-repetition-rate, sub-100-fs Ti:sapphire amplifier system," Opt. Lett. **22,** 712–714 (1997).
29. M. A. O'Leary, D. A. Boas, B. Chance, and A. G. Yodh, "Simultaneous scattering and absorption images of heterogeneous media using diffusive waves within the Rytov approximation," in *Proceedings of Optical Tomography and Spectroscopy of Tissue: Theory, Instrumentation, Model, and Human Studies II*, B. Chance and R. R. Alfano, eds., Proc. SPIE **2979,** 320–327 (1997).
30. S. K. Gayen, M. E. Zevallos, M. Alrubaiee, J. M. Evans, and R. R. Alfano, "Two-dimensional near-infrared transillumination imaging of biomedical media with a chromium-doped forsterite laser," Appl. Opt. **37,** 5327–5336 (1998).

Appendix 4

Time Sliced Three Dimensional Inverse Image Reconstruction of Objects in Highly Scattering Media

M. Xu, S. K. Gayen, W. Cai, M. E. Zevallos, M. Lax and R. R. Alfano

Institute for Ultrafast Spectroscopy and Lasers
New York State Center of Advanced Technology for Ultrafast Photonic Materials and Applications
Departments of Physics and Electrical Engineering
The City College and Graduate Center of City University of New York
New York, NY 10031

ABSTRACT

An inverse image reconstruction approach that makes use of an algorithm based on the diffusion approximation of the radiative transport theory and a sequence of picosecond-duration slices of transmitted two-dimensional (2D) light intensity distribution for fast 3D image reconstruction is presented. The results of simulation and experiment for a cylindrical geometry are presented. Object localization in the lateral dimensions is better than that in the axial direction. The observed difference in axial and lateral resolutions are analyzed by introducing the concept of "longitudinal sensitivity".

Keywords: Inverse reconstruction, time-sliced imaging, transillumination

1. INTRODUCTION

In the article, we present an inverse image reconstruction (IIR) approach that makes use of a sequence of picosecond-duration slices of transmitted two-dimensional (2D) light intensity distribution measured at one plane, instead of surrounding the medium, for fast 3D image reconstruction. This approach may allow for simpler 3D imaging of breast.

2. OPTICAL IMAGING SYSTEM

The experimental system, described in detail elsewhere,[1] makes use of $800\,nm$, $150\,fs$, $1\,kHz$ repetition-rate pulses from a Ti:sapphire laser for sample illumination and an electronic gated image intensifier coupled to a CCD camera to record time-sliced images. The scattering medium was a suspension of Intralipid-10% (Kabi Pharmacia Inc., Clayton, North Carolina) in water, adjusted to provide an estimated reduced scattering coefficient $\mu_s' = 0.4\,mm^{-1}$ and an absorption coefficient $\mu_a = 0.02\,mm^{-1}$ at wavelength $800\,nm$. The Intralipid suspension was held in a $60\,mm$ long and $200\,mm$ diameter cylindrical Plexiglas cell. The object was a $3 \times 3 \times 10\,mm^3$ rectangular parallelepiped made of aluminum and painted black. It was suspended on axis at a distance of $15\,mm$ ($z = 45\,mm$) from the exit plane. The gate width was adjusted to $80\,ps$ and time-sliced transmitted intensity distribution, $I(x, y, t_i)$, were recorded over a $5\,ns$ range by varying the gate position in steps of $100\,ps$.

3. ALGORITHM

The inverse image reconstruction algorithm is based on the diffusion approximation of the radiative transport theory for photon migration in a scattering medium. For the linear inversion case, the forward problem can be written in matrix form:

$$Y(\rho_d, \phi_d, z_d, t) = \sum_{\rho,\phi,z} W(\rho_d, \phi_d - \phi, z_d, t|\rho, 0, z) X(\rho, \phi, z) \tag{1}$$

where $Y = -\log(I/I_0)$, I and I_0 are intensities with and without the inhomogeneity respectively, $X = \Delta\mu_a c$ or $\Delta D c$ depends on the type of the inhomogeneity, and W is the weight function. The convolution over ϕ in Eq. (1) can be eliminated by a Fourier transform in the $\hat{\phi}$ direction:

$$Y_k(\rho_d, z_d, t) = \sum_{\rho,z} W_k(\rho_d, z_d, t|\rho, z) X_k(\rho, z) \tag{2}$$

Part of the SPIE Conference on Optical Tomography and Spectroscopy of Tissue III
San Jose, California • January 1999 SPIE Vol. 3597 • 0277-786X/99/$10.00

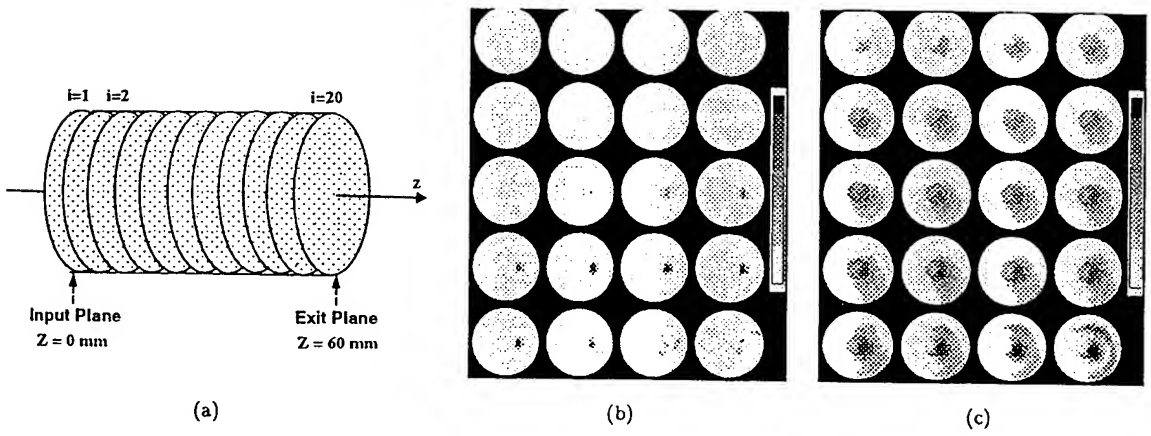

Figure 1. (a) The cylindrical slab is uniformly divided into 20 slices along the z-axis. (b) Images reconstructed from simulated data when the object was located at $z = 45\,mm$. (c) Images reconstructed from experimental data with the object located at $z = 45\,mm$. The sequence of circles represents images at $3\,mm$ intervals along the cylinder axis.

where Y_k, W_k and X_k are Fourier transforms of Y, W and X over ϕ respectively. The inverse problem is solved using a Tikhonov regularization method[2] with a diagonal form of regularization matrix $\lambda(k)$. The suitable regularization parameters $\lambda(k)$ are chosen by the L-curve criterion.[3] In our calculation, the sample cell is divided into $N_r \times N_\phi \times N_z = 10 \times 36 \times 20$ voxels. One inversion can be completed in 1 minute in a Silicon Graphics Origin200 workstation when the weight matrix is pre-computed.

4. RESULTS

4.1. Three-dimensional image from simulated data

In the simulation, we assumed a cylindrical slab of thickness $z_0 = 60\,mm$, and a disk detector of radius $R_d = 30\,mm$. The thickness of the cylindrical slab and its angle 2π was uniformly sliced into 20 and 36 parts respectively, while its radius R_d was divided into 10 parts scaled such that each voxel has equal-volume (Figure 1(a)). Sampled data both with and without hidden objects were used to obtain $Y = -\log I/I_0$ after added Gaussian distributed noise of $\pm 5\%$. The background was assumed to have a reduced scattering coefficient $\mu_s^{0\prime} = 0.4\,mm^{-1}$, and an absorption coefficient $\mu_a^0 = 0.02\,mm^{-1}$. The optical parameters of the inhomogeneity were $\mu_s' = \mu_s^{0\prime}$ and $\mu_a = 0.4\,mm^{-1}$, which was put in a voxel at the $15th$ division along z-axis.

The reconstructed image of $\Delta\mu_a$ is shown in Figure 1(b). The 20 consecutive circles in the figure represent the images at different position along the z-axis from input plane ($z = 0$) to exit plane ($z = 60\,mm$). A gray scale is used to denote the relative value of the change of the absorption coefficient. The reconstructed image locates the object in the neighborhood of where it was placed. The object appears to spread out both in the lateral and axial directions, a consequence of the scattering and the diffusion approximation used for reconstruction. The image spreads out to approximately 6-7 mm in the lateral, (ρ, ϕ) plane, and to approximately 10-15 mm along the axial, z-direction.

4.2. Three-dimensional image from experimental data

In the inverse image reconstruction using experimental data, we approximated the laser beam to be a point source located at the center of the $z = 0$ plane. The ρ boundary of the container was assumed to be infinity.

Figure 1(c) shows a 3D image of the object as a sequence of frames at $3\,mm$ intervals along the axial direction from input plane to exit plane reconstructed using experimental data. The lateral position of the object is reconstructed to be near the cylinder axis in the image map, as the actual object was placed. However, the image is spread out over approximately $20\,mm$ along the axial direction and peaked more towards the detector end than the actual object position. The worse result from experimental data indicates higher noise in experiment than 5% and existence of deviation between theoretical model and experiment.

5. LONGITUDINAL SENSITIVITY ANALYSIS

To understand why the axial resolution is poorer than lateral resolution for both simulated and experimental data, a one-dimensional model for an infinite uniform highly scattering medium with a diffusion coefficient D and an absorption coefficient μ_a was studied. A source of plane-wave pulse with intensity $S\delta(z+d)\delta(t)$ was located at $z=-d<0$, and a detector at $z=d$. An inhomogeneity in the form of an absorptive infinite layer of infinitesimal thickness Δz with diffusion coefficient D and absorption coefficient $\mu_a+\Delta\mu_a$ was placed at z where $-\infty<z<\infty$. The time-resolved fluxes received by the detector, without and with the inhomogeneity, are $I_0(t,z)$ and $I_1(t,z)$, respectively. The change of flux for an absorptive inhomogeneity is given by:[4]

$$\Delta I(t,z)=I_0(t,z)-I_1(t,z)=S\Delta\mu_a\Delta z\left\{c\int_0^t d\tau G(d,z,t-\tau)G(z,-d,\tau)\right\}, \tag{3}$$

where $G(z_1,z_2,t)$ is the one-dimensional Green's function.

We define a sensitivity function as the term inside $\{\}$ of Eq. (3) which is the change of flux measured by the detector at time t when an absorption layer of unit thickness and of unit change of absorption coefficient is placed at position z for an incident pulse of unit intensity. The sensitivity function is found to be[5]

$$W_{\inf}(t,z)=\frac{\exp(-\mu_a ct)}{4D}\operatorname{erfc}(\alpha\max(|z|,d)) \tag{4}$$

where $\alpha^{-1}=\sqrt{Dct}$ is the characteristic length. $W_{\inf}(t,z)$ is totally independent of z when the absorptive layer is between the detector and the source. Therefore, for one-dimensional case, reconstruction using only transmission measurements is not sensitive to axial position of the inhomogeneity. In a 3D transmission case, such as that in section 3, it is not so severe but limits the longitudinal resolution, as we have observed in section 4.

6. CONCLUSION

An inverse image reconstruction approach that uses a sequence of time slices of two-dimensional light intensity distribution, and a fast algorithm based on the diffusion approximation of the radiative transport theory is presented. Results of reconstruction with simulated and experimental data are also presented. The image spreads to about 6-7 mm in the lateral, and to approximately 10-15 mm along the axial direction for one voxel inhomogeneity in simulation while the image spreads out to approximately 20 mm along the axial direction for experimental data. The difference in lateral and axial resolutions may be explained by the concept of "longitudinal sensitivity".

ACKNOWLEDGMENTS

This work is supported in part by National Aeronautics and Space Administration, Department of Energy, US Army Medical and Materials Research Command, Mediscience Technology Corp. and New York State Science and Technology Foundation.

REFERENCES

1. W. Cai, S. K. Gayen, M. Xu, M. Lax, and R. R. Alfano, "Inverse reconstruction of three-dimensional tomographic images of objects in turbid media from time-sliced two-dimensional transmission measurements," in *Advances in optical and photon migration*, J. G. Fujimoto and M. S. Patterson, eds., vol. 21 of *OSA TOPS*, pp. 138–141, 1998.
2. A. N. Tikhonov, "On the solution of incorrectly stated problems and a method of regularization," *Dokl. Akad. Nauk SSSR* **151**, pp. 501–504, 1963.
3. P. Hansen and D. O'Leary, "The use of the L-curve in the regularization of discrete ill-posed problems," *SIAM J. Sci. Comput.* **14**, pp. 1487–503, November 1993.
4. S. R. Arridge, "Photon-measurement density functions. part I: Analytic forms," *Appl. Opt.* **34**(31), pp. 7395–7409, 1995.
5. M. Xu, W. Cai, M. Lax, and R. R. Alfano, "Locating an absorptive layer using optical diffusion tomography: analytically solvable one-dimensional transmission and backscattering models," *Opt. Lett.* , submitted.

4

Appendix 5

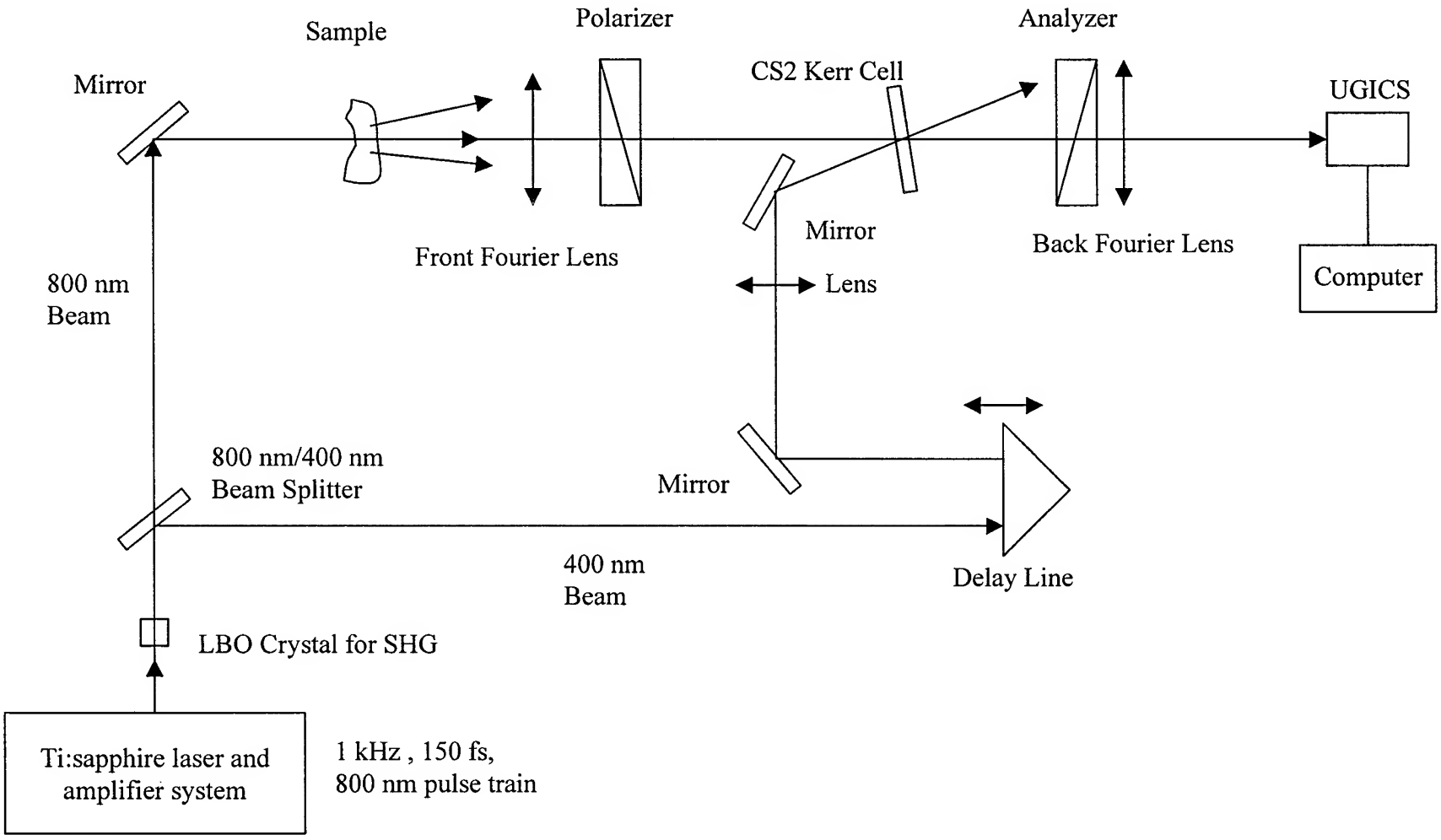

Fig. A schematic diagram of the time-sliced imaging arrangement with an optical Kerr gate using a Ti:sapphire laser

Appendix 6

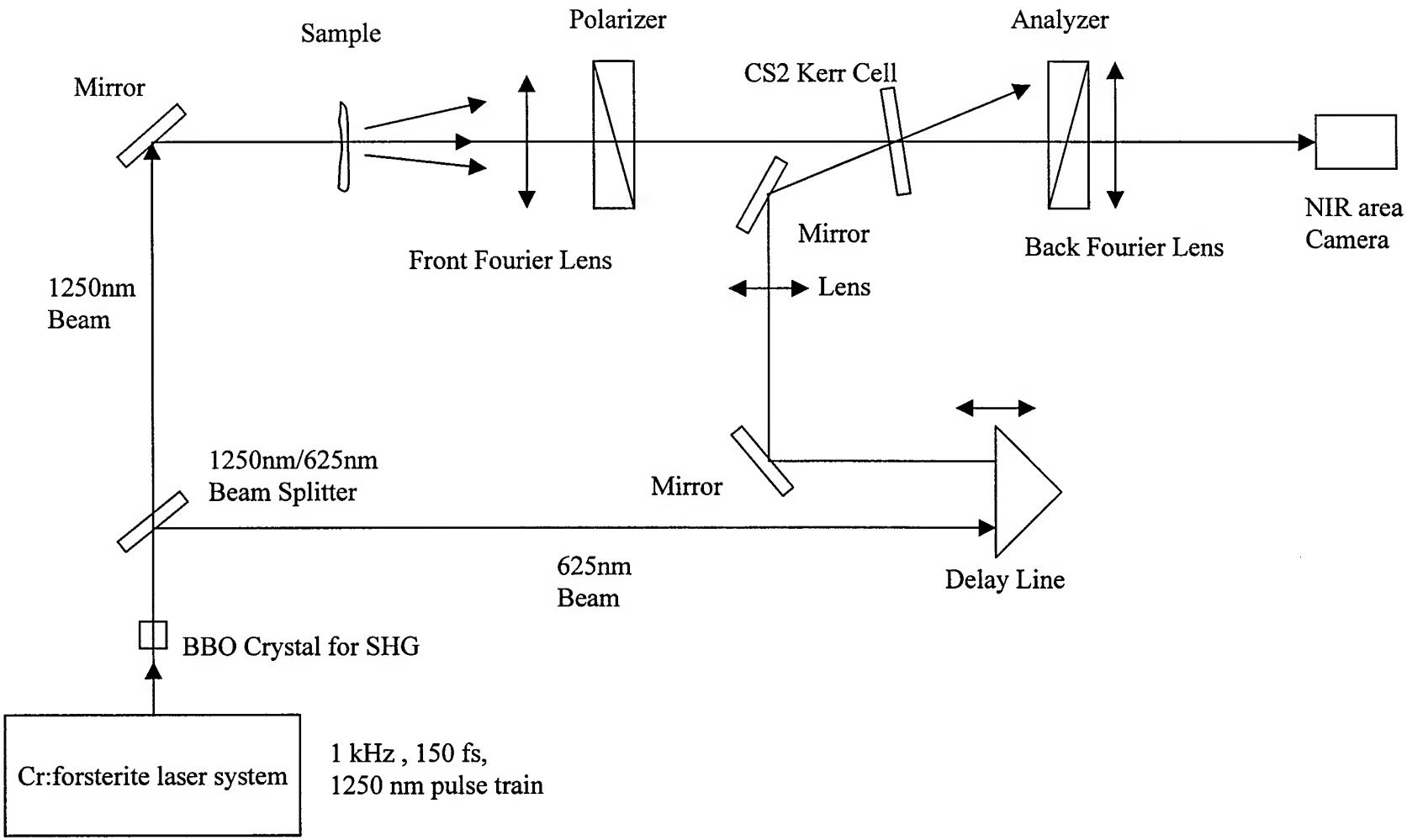

Fig. A schematic diagram of the time-sliced imaging arrangement with an optical Kerr gate using the Cr:forsterite laser

Appendix 7

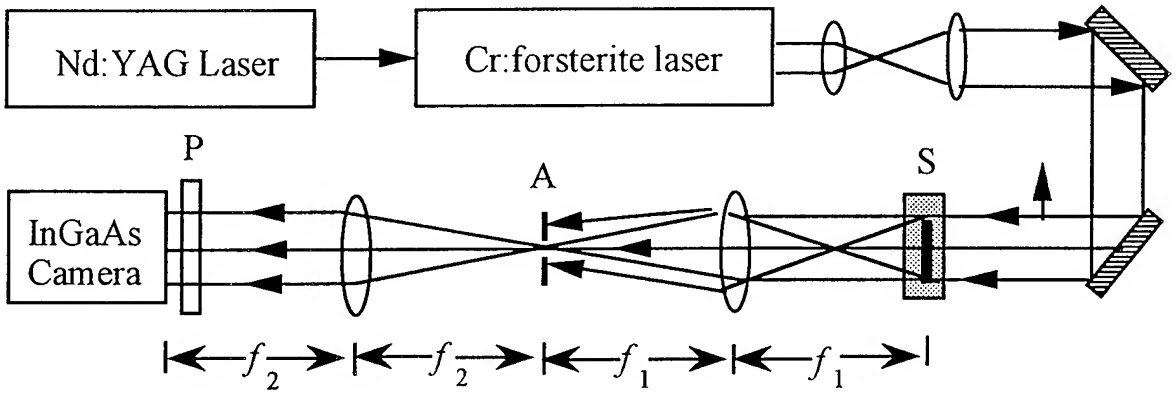

Fig. A schematic diagram of the experimental arrangement for spectroscopic imaging. (A = aperture; P = polarizer; S = sample)